

Identifying the regulatory role of small molecule in cancer phenotypes

A Thesis submitted to

Indian Institute of Science Education and Research Pune in partial fulfillment of the requirements for the BS-MS Dual Degree Programme

by

SWATI CHOUDHARY

20151016



Supervisor: Prof. Sudhir Krishna

Co-Guide- Dr. Sanjukta Mukherjee

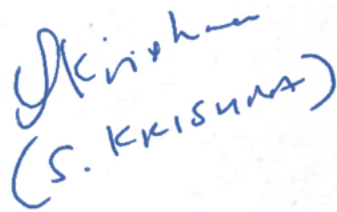
National Centre for Biological Sciences, Bangalore, Karnataka,
India

TAC - Prof. Sanjeev Galande

Certificate

This is to certify that this dissertation entitled “**Identifying the regulatory role of small molecule in cancer phenotypes**” towards the partial fulfilment of the BS-MS dual degree programme at the Indian Institute of Science Education and Research, Pune represents study/work carried out by “**Swati Choudhary at National Centre for Biological Sciences, Bangalore India**” under the supervision of “**Prof Sudhir Krishna, Professor, Department of Cellular Organization and Signalling, National Centre for Biological Sciences**” during the academic year **2019-2020**.

Committee:



A handwritten signature in blue ink that reads "S. Krishna" with "(S. KRISHNA)" written below it in parentheses.

Supervisor: Prof. Sudhir Krishna

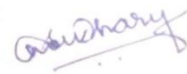


A handwritten signature in black ink that reads "Sanjeev Galande".

TAC: Prof. Sanjeev Galande

Declaration

I hereby declare that the matter embodied in the report entitled “Identifying the regulatory role of small molecule in cancer phenotypes” are the results of the work carried out by me at the **Department of Cellular Organization and Signalling, National Centre for Biological Sciences**, under the supervision **Prof. Sudhir Krishna** and the same has not been submitted elsewhere for any other degree.



Swati Choudhary

01-04-2020

Acknowledgements

I would like to express my sincere gratitude to my supervisor, Prof. Sudhir Krishna and my co-guide Dr. Sanjukta Mukherjee at NCBS-TIFR, Bangalore. I am extremely thankful to my co-guide Dr. Sanjukta Mukherjee for having immense faith in my abilities and whose expertise was invaluable in the formulating of the research topic in particular. I am thankful to you for your constant support and guidance throughout my thesis project and for considering my ideas and allowing to pursue them every time. I would like to acknowledge Indian Institute of Science Education and Research, Pune for providing the wonderful opportunity to carry out research at NCBS-TIFR.

I am really thankful to Stabonia Maji for her constant guidance throughout my thesis work. I would like to thank Nayim Paul for his constant help during the experiments. I convey my gratitude towards Prof. Krishnamurthy for training me to use the Flow cytometry facility. I would like to thank Prof. Akash Gulyani for letting me use the microscopic facilities of his lab. I would also like to acknowledge my colleagues from my project workplace and IISER-P for their constant support. I would like to convey my gratitude towards Prof. Sanjeev Galande Laboratory of Chromatin Biology and Epigenetics, Indian Institute of Science Education and Research, Pune for being my TAC member. In addition, I would like to thank my parents and my brother Abhishek Choudhary for their wise counsel and sympathetic ear. Finally I would like to thank Jyothish Sudhakaran, Annirudh Pillai and my previous mentor from Sanjeev's lab Ankita Sharma for helping me and giving me valuable comments to make my thesis better.

ABBREVIATIONS

Acronym	Full Form
cDNA	Complimentary DNA (Deoxyribonucleic Acid)
CMBL	Cyclic Mismatch Binding Ligand
DMEM	Dulbecco's Modified Eagle Medium
DMSO	Dimethyl Sulphoxide
DNA	Deoxyribonucleic Acid
dNTP	Deoxyribonucleotide triphosphate
EMT	Epithelial to Mesenchymal Transition
FBS	Fetal Bovine Serum
HaCaT	Human Keratinocyte Cells
HEPES	4-(2-hydroxyethyl)-1-piperazineethanesulfonic acid
HPV	Human Papilloma Virus
miR	MicroRNA
mRNA	Messenger RNA (Ribonucleic Acid)
PBS	Phosphate Buffer Saline
PenStrep	Penicillin Streptomycin
pre-miR	Precursor microRNA (Ribonucleic Acid)
pri-miR	Primary microRNA (Ribonucleic Acid)
RNA	Ribonucleic Acid
SELEX	Systematic evolution of ligands by exponential enrichment
siRNA	Short interfering RNA (Ribonucleic Acid)
TE	Trypsin EDTA (Ethylenediaminetetraacetic acid)
PI	Propidium Iodide
7-AAD	7-Aminoactinomycin D
PE	Phycoerytrin

Table of Contents

Sr. No.	Contents	Page No.
1.	Abstract	7
2.	1. Introduction	8-12
	1.1 Part I: Screening of CMBLs (21 analogues) using scratch wound healing cell migration assay	13
	1.2 Part II: Evaluation of regulatory role of telomere DNA binding CMBLs on cancer phenotype	14-21
3.	2. Methods and materials	22-30
4.	3. Results and Discussions	
	3.1 Screening of CMBLs (21 analogues) using scratch wound healing cell migration assay	31-32
	3.2 Categorization of CMBLs into three parts based on the cells ability to invade the empty spaces	32-39
	3.3 CMBL7b and CMBL3a is cytotoxic for human cervical cancer cell line CaSki with little effect on Normal Human keratinocytes HaCaT	40-41
	3.4 Dose dependent treatment of CMBL7b in cervical cell line CaSki induces apoptosis	42-44
	3.5 CMBL3a (7 μ M) induces apoptosis post 24 hours treatment in cervical cancer cell line CaSki	44-46
	3.6 CMBL7b induces cell cycle arrest in cervical cancer cell line CaSki	47-49
	3.7 CMBL3a induces cell cycle arrest in cervical cancer cell line CaSki	49-51
	3.8 Clonogenic growth inhibition by CMBL7b and CMBL3a	51-53
5.	Conclusion and Future perspectives	53-54
6.	References	55-57

Identifying the regulatory role of small molecules in cancer phenotypes

ABSTRACT: Cancer developing to metastatic progression is one of the causes of lethality. In biomedical research, small molecules that modulate cell migration have great potential as anti-cancer agents and may be of direct therapeutic importance, since both tumor angiogenesis and metastasis depend on cell migration. However anti-migratory compounds are presently limited. Furthermore, there is a growing interest, in the potential benefit of combining phenotypic and targeted approach, in the quest to advance small-molecule drug discovery. Cyclic Mismatch Binding Ligands (CMBLs) are recently developed a novel class of small molecule. Anti-cancer activities of CMBLs are yet not examined. Evaluation of the effect of CMBL on cancer phenotypes along with its cellular target would provide a deeper insight into the potential of CMBL as anti-cancer drug candidates. Towards this goal in first part of my study we categorized 21 CMBL analogues with respect to their ability to regulate cell migration using metastatic cervical cancer cell line CaSki by wound healing assay. Binding based screening approach using SPR already revealed the affinity for few CMBL analogues (CMBL3a and 7b) towards cellular nucleic acid target such as telomere DNA repeat. Wound healing assay already indicated the inhibitory effect of CMBL3a and 7b on CaSki cell migration. In second part of the study we evaluated the regulatory role of CMBL3a and 7b on cell cycle and other cancer phenotypes such cell proliferation, apoptosis and colony formation. Results suggests different modes of action for these two compounds in suppressing tumor cell growth indicating an intriguing possibility of multiple putative targets for efficiently treating tumor cell proliferation and metastases.

1. Introduction

Drug Discovery strategies: Drug discovery for cancer like any other therapeutic areas have typically been used two preclinical strategies (i) phenotypic drug discovery (PDD) and (ii) target-based drug discovery (TDD) to identify potential drug candidates (D.C. Swinney et al., 2013, Daniel Gandia, 2019, Yoo-Ah et al., 2016, John G. Moffat et al., 2014).

Phenotypic drug discovery (PDD): PDD involves phenotypic screening to identify molecules with the ability to exert the desired effects on cancer cell's phenotype. Phenotypes are an organism's observable characteristics in authentic biological systems such as animals or cells. In cancer PDD involve some phenotypic assays that measure proliferation, differentiation, migration and other cancer phenotypes. Historically, phenotypic screening has a slight advantage and many of the today's fast-in-class drugs were discovered through phenotypic screening. However, a recent article concluded very few drugs were discovered entirely by 'classical' PDD and most of the discovery used combined approach of phenotypic and target-based assay. PDD based strategy is advantageous to identify active compound in cellular phenotype context and attributed to the lack of bias when it comes to identifying a drug's mechanism of action. However, despite the considerable advancement in phenotypic cell-based screening tools, there are still challenges associated with this approach such as its specificity in cellular context, actual mechanism of the drug's action often determined later, and sometimes not for many years so on (D.C. Swinney et al., 2013, Daniel Gandia, 2019, Yoo-Ah et al., 2016, John G. Moffat et al., 2014, David C. et al., 2011).

Target-based drug discovery (TDD): In the post genomic era TDD based drug discovery is an emerging field in past two decades which are predominantly hypothesis-driven and referred to as target-based. It focuses on discovery and development of drug candidates to treat unmet medical need by targeting specific molecular pathway or gene products, such as mutations, defects at specific

molecular locations in human that associated with some cancer pathogenesis and specifically proteins that appear to have a key role in disease pathogenesis. It mounts the hope of developing successful therapies for personalized medicine also. According to literature significant numbers of approved drugs or investigational cancer drug candidates are classified as targeted and the majority of which (21 out of 29) are kinase inhibitors such as imatinib (Gleevec), gefitinib (Iressa) and erlotinib (Tarceva) (Khushwant S. Bhullar et al., 2018).

Advantages and Disadvantages of PDD and TDD: Both targeted and classical phenotypic cancer drug discovery possesses substantial challenges. Although empirical phenotypic approaches use semi empirical methods that do require an understanding of biology to certain extent but understanding of the mechanism is not essential. It may slow down the progression of the drug candidate because subsequent studies such as some understanding of mechanism to help evaluate dose-response relationships will need to be empirical and added the additional cost as well. Similarly, it has been revealed from previous report, a target-based discovery partly reflects the lower productivity due to the lack of consideration of the molecular complexities of the drugs' action. So, the requirement for the evaluation of multiple hypotheses will add to the cost of development as well in the case of target-based approach. Many factors influenced the shift from a classical phenotypic approach to a target-based approach, such as it uses chemistry, informatics and molecular tools of genetics to drive drug discovery and also provide criteria and boundaries for choosing patient populations, setting doses, and quantitatively measuring efficacy and toxicity. Despite the substantial increase in the rate of investment in R & D, there is no increase in the rate of discovery of truly innovative new drugs that has approved by Search Results Web result with site links U.S. Food and Drug Administration (FDA) (Behzad Mansoori et al., 2014, Keita Uchino et al., 2013, Weige Tan et al., 2018). There is a growing interest, in the potential benefit of combining phenotypic and genomic data for targeted approach, in the quest to advance small-molecule chemical probe and/or drug discovery (Khushwant S. Bhullar et al., 2018).

The challenge is to use an appropriate combination of emerging targeted approach and classical phenotype screening to enable good ideas to successfully move forward to identify and develop novel drug candidates.

Cyclic Mismatch Binding Ligands (CMBLs): Cyclic Mismatch Binding Ligands (CMBLs) are a recently developed novel class of small molecules that belongs to class cyclophanes, it contains two heterocycles having a nucleobase recognition hydrogen-bonding surface connected by two linkers (Linkers A and Linkers B) (Figure 1a-e). (Sanjukta Muherjee et al., 2016, Sanjukta Muherjee et al., 2017, Sanjukta Muherjee et al., 2017, Sanjukta Muherjee et al., 2019).

Linkers provide conformational restrictions to the dynamic motion of the two heterocycles, it also provides the limited conformational flexibility or pre-organization of two heterocycles and hence the orientation of its H-bonding surface. CMBLs were designed rationally with the hypothesis “the pre-organized conformation might improve the target specificity of the ligand for its exploration in the complex biological systems”. CMBLs were rationally designed to target specific structure/sequence of nucleic acids (DNA and /or RNA). So far developed CMBL library, comprises 21 novel class of small molecules that contains two heterocycles typically 2-amino 1,8-naphthyridine moieties linked by variable linker A (at c-2 position) and linker B (at c-7 positions) (Figure 1a-e). 2-amino 1,8-naphthyridine moiety of CMBL comprises H-bonding surface complementary to the guanine (Figure 1b). CMBL4 (or 4a) was the first reported molecule belonging to class CMBL (Sanjukta Muherjee et al., 2016). Sequence specific binding study of CMBL4 with duplex DNA having bulge-mismatch (T/GG) sequence was first reported at 2016 (Figure 1b). In 2017 reported the molecular diversity of CMBLs, which allowed the tuning of the binding affinity and selectivity of the CMBLs towards non-canonical duplex DNA/RNA and different biologically significant repeat DNAs by linker variation (Sanjukta Muherjee et al., 2017).

A recent paper reported the structural insights of one CMBL analogues targeting A–A pairs in disease-related CAG RNA repeats. (Sanjukta Muherjee et al., 2019) Previous studies on CMBL analogues and its target identification using different *in vitro* methods revealed its affinity towards diverse biologically relevant DNA and/or RNA sequence. A Systematic Evolution of ligand by Exponential Enrichment (SELEX) based *in vitro* studies revealed the binding of one CMBL analogues to pre-mir-24, which is seen to be upregulated in several cancers including cervical cancer (unpublished work by M. Sanjukta et al.). Similarly, surface plasmon resonance (SPR) based screening approach revealed the binding affinity of few CMBL analogues (CMBL3a and CMBL 7b) (Figure 1d and e) towards telomere DNA repeat sequence [d(TTAGGG)_n] (performed By Malavika Pillai). Further studies done by a previous student Stabonia Maji (one-year CSIR-JRF) on the compound CMBL3a revealed that it was regulating the G2/M phase of cell cycle (unpublished work).

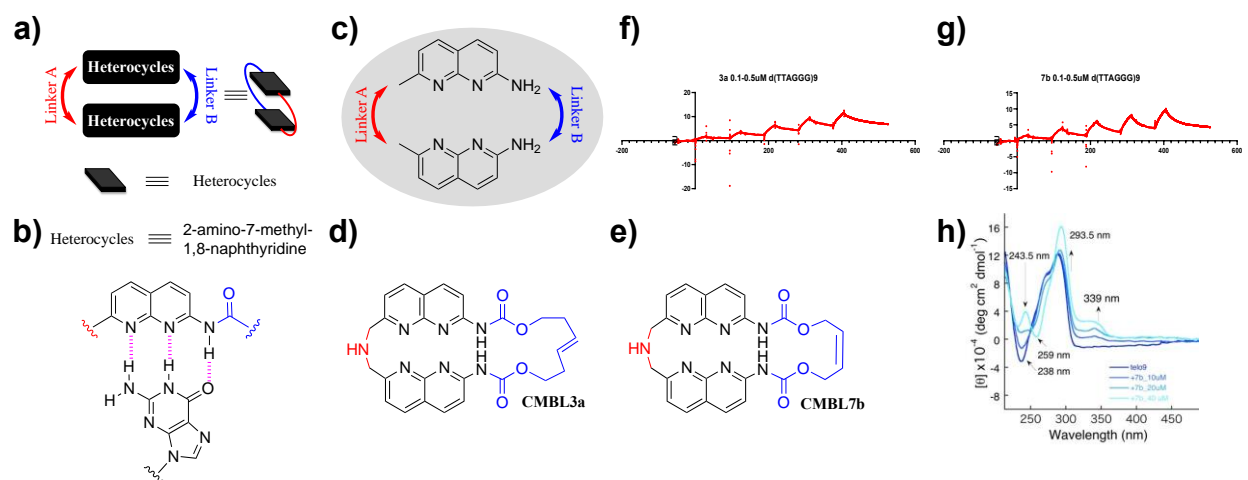


Figure 1(a) General structure of CMBLs (where two heterocycles attached by two linkers; **(b-c)** So far developed CMBLs comprises two 2-amino-1,8-naphthyridine moiety that has H-bonding surface complementary to guanine (b) and attached by two linkers (c); **(d-e)** chemical structure of CMBL3a (d) and CMBL7b (e); (f-g) Single-cycle kinetics (SCK) surface plasmon resonance (SPR) analysis of the CMBL3a and CMBL7b with telomere repeat DNA [d(TTAGGG)₉ (telo9)], immobilized (immobilization RU 612) on series S SA sensor surface. Ligands were added sequentially to 0.1, 0.2, 0.3, 0.4 and 0.5 μM . (f) CD spectrum of d(TTAGGG)₉ (telo9) (2.5 μM each) were measured in Tris-HCl buffer (25 mM, pH 7.5) and KCl (100 mM) at 25 °C with increasing concentration of CMBL7b (0, 10, 20 and 40 μM). SPR analysis and CD analysis were performed by Malavika Pillai (short term intern).

Evaluation of the effect of CMBL on cancer phenotypes along with identification of its genomic target would give a better picture to evaluate the potential of CMBLs as an anti-cancer drug candidate. Toward this goal my project work was divided into two parts:

Part I: Screening of CMBLs (21 analogues) using scratch wound healing cell migration assay

Part II: Evaluation of regulatory role of telomere DNA binding CMBLs on cancer phenotype

Part I: Screening of CMBLs (21 analogues) using scratch wound healing cell migration assay

Indicated by the 2018 estimates and incidences of cervical cancer, it was seen that cervical cancer is the second most prevailing cancer among women worldwide (Arbyn M et al., 2018). Metastasis remains the primary cause of cancer related deaths worldwide (Nicolo Riggi et al., 2018). This is because of the lack of drug targeting the metastatic progression. Due to the significant improvements made in early detection and treatment for primary tumors, cancer survivals have been significantly increased. But there are no such advancements made for metastatic cancer that is the advanced stage of malignancy. Metastasis is mainly the result of cell dissemination resulting from the detached tumor cells from the basement membrane and its ability to migrate and invade the other body parts by dynamic re-organization of cytoskeleton proteins and molecular alternation. (Prem Prakash et al., 2019)

The initial steps of cell migration at single cell level involves five-step processes

1. Formation of a leading-edge protrusion that marks the rear end of the cell by changing the cytoskeleton structure by actin polymerization.
2. Engagement of extracellular substrates and adhesion of cell surface receptors to the leading-edge protrusion to generate the force for movement.
3. Behind the leading edge, the cell surface proteases become engaged with the extracellular scaffold proteins and there is localized proteolysis
4. Actomyosin contraction generates tension inside the cell due to the activation of myosin ii by Rho GTPase
5. The cell moves forward by the slow turnover of the adhesion bonds at the trailing edge of the cell

Part II: Evaluation of regulatory role of telomere DNA binding CMBLs on cancer phenotype

Telomere repeat structure and function: DNA is the molecular target for many anticancer drugs (Julia R. Pon et al., 2015). Telomere DNA length and telomerase activity plays a crucial role for cancer initiation and for the survival of tumors (Viay Sekaran et al., 2014, Mohammad A. Jafri et al., 2016, Jerry W. Shay et al., 2016).

Genomic stability in eukaryotes is maintained by telomere for its proper functioning. Telomeres consists of noncoding tandemly repeating hexanucleotides DNA sequences $d(\text{TTAGGG})_n$ (5'→3' direction) located at the extreme ends of the chromosome (Figure 2a). It comprises 2–20 kb of double-stranded TTAGGG repeats and terminating in a single-stranded G-rich overhang of 50–500 nucleotides at the ends of chromosome (Figure 2b, e) [22-26]. Telomeres are structurally and functionally complex. The G-strand overhang forms the t-loop in which it invades the double-stranded region (Figure 2b). It has been hypothesized that those structures, which can sequester the 3' end, prevent the extension of the telomeres by telomerase. G-rich single stranded telomeric DNA form specialized four-stranded helical structures that involve Hoogsten-type base pairing between four guanines, named G-quadruplex (or G4) (Figure 2b, e) (Yan Xu., 2011).

These double-stranded repeats have one guanosine-rich strand (G-strand) copied by the lagging- strand replication, and one cytosine-rich strand (C-strand) synthesized by leading-strand replication. Their main function is to protect and confer the stability to chromosome ends (Figure 2c, d). It acts as a cap for protection from enzymatic degradation, protects from unnecessary recombination, repair, interchromosomal fusion, and maintains the integrity of the internal regions of the chromosomes. The number of repetitions in the telomere varies widely among different organisms and also among different telomeres in one organism. For example, tetrahymena has $d(\text{TTGGGG})_n$ and for all vertebrates, including humans, the repetitive sequence is $d(\text{TTAGGG})_n$. In humans, these repetitive sequences are 15 - 20 kb in length at birth and about 8 - 10 kb in adults (Viay Sekaran et al., 2014, Mohammad A. Jafri et al., 2016).

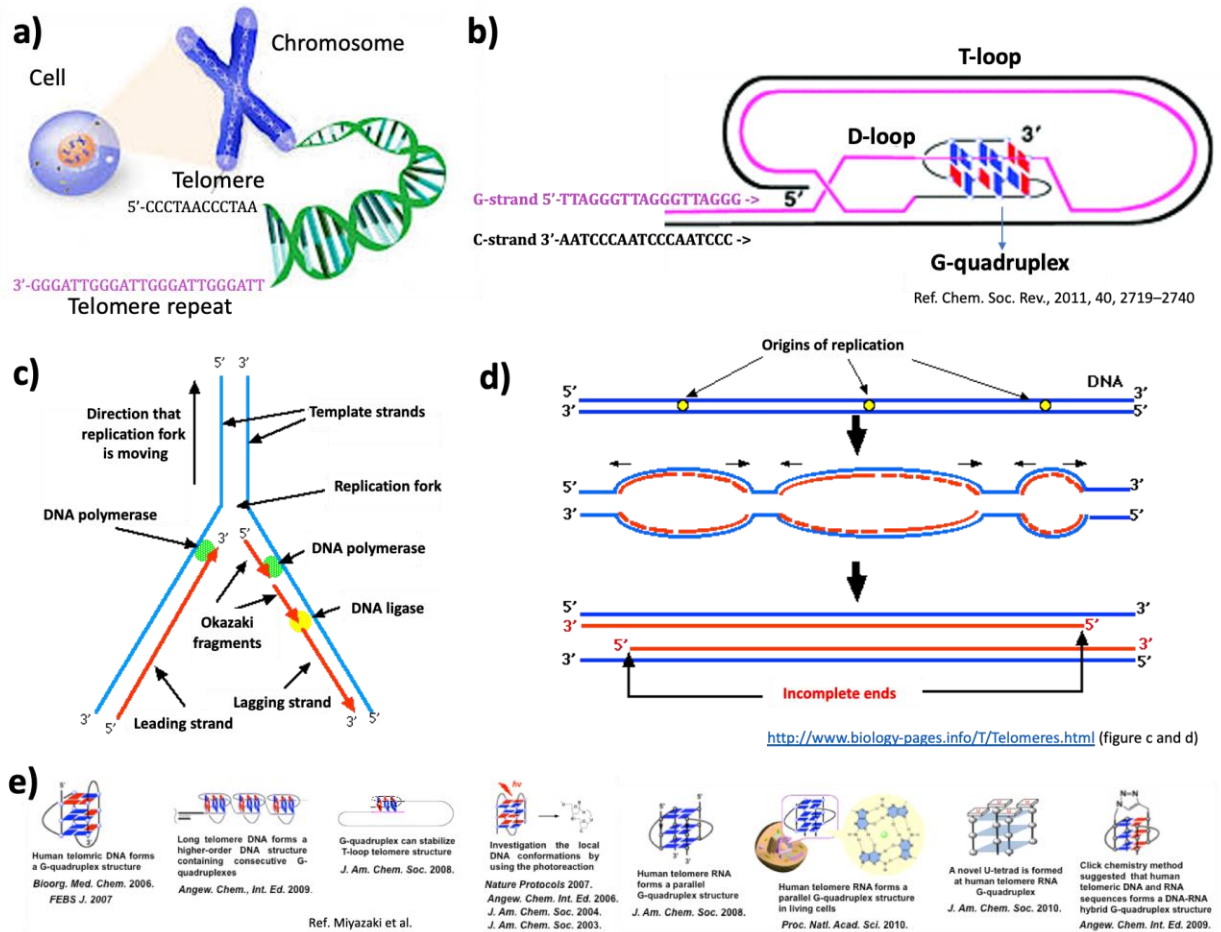


Figure 2. (a) structure of chromosome with telomere repeat at the (5' to 3') end; (b) T-loop, D-loop and G-quadruplex structure of telomere DNA. A segment containing 16-mer G-tracts can bind to the G-tract of another segment of telomere DNA by forming G-quadruplex when the 30 - end invades the adjacent double-stranded segment of the telomere to form the t-loop. (c-d) Mechanism of DNA replication and formation of single stranded overhang telomere repeat DNA strand. (e) High ordered structure of telomere repeat DNA.

The mechanism of DNA replication is different for the leading and the lagging strand. The leading strand gets replicated continually but lagging strand replication starts by DNA polymerization from multiple RNA primers which are elongated to create Okazaki fragments. The RNA primers at last get replaced by the DNA sequences. The terminal RNA primer creates a gap and the last strand cannot be synthesized to its end as there is no template for the last Okazaki fragment beyond the 5' end of the chromosome (Figure 2c, d). In normal somatic cells telomere gets shortened by each round of the DNA replication due to the end replication problem and cells with excessive

sort telomere undergoes p53 dependent apoptosis or senescence induced by the DNA damage response. The somatic cell lineage can undergo limited number of populations doubling due to the telomere shortening leading to blockage of proliferative expansion. However, the embryonic stem cells and cancer cells overcomes this problem of telomeres shortening by maintaining the telomere lengths to acquire immortality (Viay Sekaran et al., 2014, Mohammad A. Jafri et al., 2016).

According to the previous studies two mechanisms of the telomere shortening have been discovered. The first one is through the telomere reverse transcriptase which is also known as telomerase and the second one is through alternative lengthening of telomere (ALT), it uses the telomerase-independent telomere maintenance mechanism utilizing the DNA homologous recombination repair pathway. The human telomerase transcriptase is expressed in the 85-95% of the cancer cells; there it gives the property of limitless proliferation whereas the ALT pathway activation is seen in 5-15% of the cancer cells. (Masood A. Shamma, 2011, JerryW. Shay et al., 2016).

Telomerase and Shelterin proteins (Tosome): Telomerase, a specialized ribonucleoprotein reverse transcriptase the enzyme important for the maintenance of telomeres length. It is transcriptionally repressed and is not usually active in most of the human somatic cells (cells of the body) unlike mouse somatic cells, which are mostly telomerase positive. It is also active in germ cells and some adult stem cells. Human telomerase (specifically biologically active human telomerase) enzyme contains two major components, a telomerase reverse transcriptase (TERT) and a telomerase RNA (TR or hTR or TERC) (Figure 3a, b), and several additional proteins, such as two dyskerin–NHP2–NOP10–GAR1 complexes bound to the two hairpin stems of the hTR hairpin-hinge-hairpin–ACA (H/ACA) motif; and a WD40-domain protein, TCAB1 (also known as WDR79 or WRAP53 β), bound to the 3' hairpin loop. The protein TERT is highly conserved across different species, and it usually contains four major functional domains: the TERT N-terminal domain (TEN), the TERT RNA binding domain (TRBD), the reverse transcriptase domain (RT), and the C-terminal extension. The TEN domain interacts with the ss telomere DNA repeats, the TRBD domain binds multiple sites of TR, and the RT and C-terminal extension domain binds the RNA/DNA hybrid and

catalyzes the addition of DNA repeats onto the 3' end. In contrast to the relatively conserved TERT, TRs differ greatly not only in sequence but also in length. Studies revealed a conserved secondary structure among TRs across different species, which includes a 5' template boundary element, a pseudoknot, a loop-closing helix, a stem terminus element (STE), and a large loop containing the template. The conservation of secondary structures rather than sequences suggests the role for these RNA structural motifs in telomerase function, and indeed, these regions of TR are essential for synthesis of telomere repeats (Figure 3a, b) (Mohammad A. Jafri et al., 2016, Jerry W. Shay et al., 2016).

Apart from it telomeric DNAs are also bound by shelterin protein complexes. These sheltering proteins play an important role in protecting the telomeres from DNA repair mechanisms in many eukaryotes and to regulate telomerase activity as well. Shelterin has six subunits: Telomeric repeat factors 1 and 2 (TRF1 and TRF2), Protection of telomeres 1 (POT1), Repressor/activator protein 1 (RAP1), TRF2-interacting nuclear protein 2 (TIN2), and TIN2-interacting protein 1 (TPP1) (Figure 3a, b) (Raffaella Diotti et al., 2011).

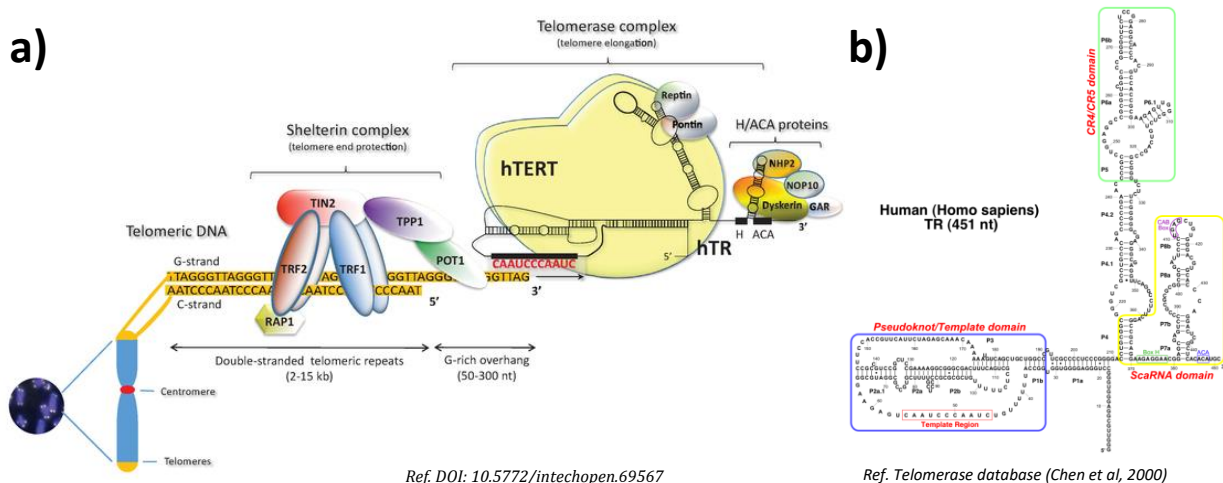


Figure 3 (a) The human telomere ribonucleoprotein complex with telomerase and shelterin protein. The human telomerase complex is composed of of telomerase reverse transcriptase (hTERT), telomerase RNA component (hTR), and accessory proteins that are members of the H/ACA small nucleolar ribonucleoprotein family: dyskerin; NHP2 (non-histone protein 2); NOP10 (nucleolar protein 10); GAR1 ribonucleoprotein. (b) Secondary structure of human (Homo

sapiens) telomerase RNA component (hTR) comprises template region (shown in red box) that has complementary sequence with telomere repeat DNA.

Telomere-driven diseases: Telomere shortening is the cause of cancer, aging and most of the age-related diseases. Different telomere targeted diseases gets triggered by the chromosomal instability that is caused by the shortening of the telomeres. Telomere depletion is closely related to cell senescence. Diabetes, coronary heart disease, psychological stress, hormones, and high blood pressures are all risk factors to accelerate telomere shortening (Figure 4a-c) (Martinez P et al., 2017, (Stephanie Wang et al., 2019).

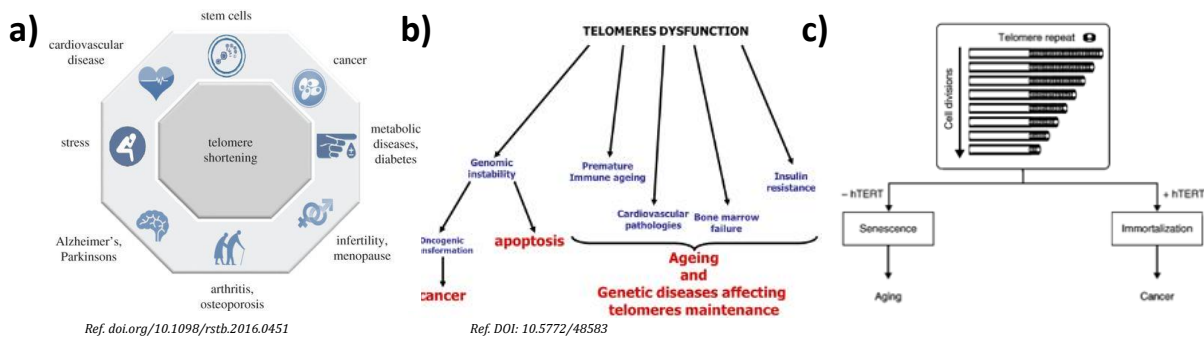


Figure 4 Telomeres dysfunction and associated diseases

Cancer and telomere: Telomere shortening is the characteristic of normal cells and only in the cells that need to maintain an active proliferative and renewal potential have the upregulation in the telomerase activity that is essential for maintenance of telomere length. Primarily tumors are likely to occur in the cells having telomere shortening. For survival of tumor cells it is necessary for the tumor cells to maintain the telomerase activity. Critically, short telomeres have been reported to be common and prevalent in early genetic alterations in cancer initiation. Short telomeres are potentially recognized as double stranded breaks (DSBs), leading to induction of the DNA damage response machinery and activation of DNA damage repair through the NHEJ pathway, resulting in end-to-end chromosomal fusions. When cells with fused chromosomes enter subsequent mitotic cycles, these chromosomal fusions are likely to break and result in chromosomal aberrations. Repeated breakage–fusion–bridge cycles cause

accumulation of chromosomal instability that serves to fuel malignant transformation. Studies using telomerase deficient mice (mTER) have revealed that the loss of telomeres is correlated with an elevated frequency of cytogenetic abnormalities (end-to-end chromosomal fusions). This is further supported by other studies using telomerase and p53 double-knockout mice in which increased genomic instability, characterized by the accumulation of dicentric chromosomes and an inclination toward oncogenic transformation, is observed. These observations are in line with the long-hypothesized role of telomere shortening as a powerful tumor-suppressive mechanism (Figure 2a-c) (Masood A. Shamma, 2011, Prasad et al., 2020). Telomerase activation, which is very important for cell immortalization, has been proposed as a critical step for the development of different types of cancer including cervical cancer. Telomere length and telomerase activity has adverse effect on cancer phenotypes. Infinite proliferation capacity is one of the unique features of cancer cells which are accomplished by maintaining telomere length at the chromosome ends through the activation of human telomerase [hTERT].

Apoptosis is a process marked by the distinct morphological and biochemical changes leading to programmed cell death (Rafael Solana et al., 2004, Maria Teresa Ventura et al., 2017). One of the structural and functional changes that occur during apoptosis is the modulation of telomere length and telomerase activity. Production of reactive oxygen species as a consequence of mitochondrial dysfunction is one of the early events of apoptosis and is related to telomere shortening (Kuhlow D et al., 2010). Cellular senescence is the progressive and irreversible loss of proliferative potential of cells. This phenomenon is characterized by a loss in replicative capacity and a series of dramatic changes in cell morphology, gene expression, epigenetics, metabolism, and others. As human cells proliferate in culture and their telomeres get progressively shorter, leading to an irreversible growth arrest leading to cellular senescence. Telomere length and telomerase activity also involve in regulation of cell cycle. Cell cycle involves the duplication of the DNA content before the cell division and this progression is tightly regulated process and is associated with cell proliferation and differentiation. Telomere shortening and inactivation of cell cycle check is identified as a

hallmark feature that characterizes the transition of premalignant to malignant lesions (Norbury CJ et al., 2001). Due to extreme shortening, telomere loses its capping function leading to induction of DNA damage response by p53-p21 pathway and permanent cell cycle arrest (Lowe SW et al., 2000). These DNA damage checkpoints are regulated by upstream protein kinases ATM and ATR and downstream kinases CHK1 and CHK2 (d'Adda di Fagagna F et al., 2003).

Telomere targeting therapies in cancer:

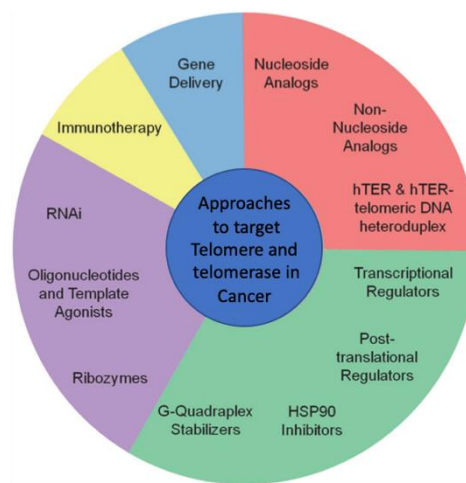


Figure 5.a five different approaches to target telomere and telomerase for the development of the telomere targeted cancer therapy

Telomere and telomerase are a well validated target for the development of anticancer drugs. Diverse approaches have been adopted to achieve this goal (Figure 5). Such as the development of antisense oligonucleotides and small nucleotide inhibitors. The therapeutic strategies include targeting telomeric cap, telomerase hTR, G-quadruplex structure of telomere DNA and other (Bartkova J et al., 2005). There are several academic and pharmaceutical groups that have initiated programs to discover small molecule that regulate telomere or telomerase activity. Small molecule-based

approaches to regulate telomere or telomerase included repurposing of viral reverse transcriptase inhibitors, natural products screening, high throughput screens of diverse compound libraries and recently emerging structure-based discovery and optimization. The most advanced area of small-molecule drug discovery involves identification or development of G-quadruplex-telomere DNA stabilizing ligands (d'Adda di Fagagna F et al., 2003). As described above telomere DNA structures are heterogeneous with a variety of structural topologies (Figure 2e) that could be a good drug target. For the last decade, considerable research has been focused on small molecules having extended planar aromatic moieties, that intercalate into G-quadruplexes and form a stable conformation. Disubstituted anthraquinone derivatives were the first G-quadruplex ligands explored as telomerase inhibitors. Since this time several studies focus on other polycyclic heteroaromatic scaffolds, macrocycles naturally available small molecules such as berberine, sanguinarine, and others (d'Adda di Fagagna F et al., 2003). One of the most significant recent advances toward selective G-quadruplex targeting is the ability to rationally design molecules using structure-based approaches. Despite these efforts, small molecule telomere inhibitors have yet to reach the clinic (Mohammad A. Jafri et al., 2016, JerryW. Shay et al., 2016, Stephanie Wang et al., 2019). The more challenging hurdle that still remains is to using these molecules is cytotoxicity due to non-specificity leading to other side effects, poor pharmacokinetic and pharmacodynamic properties. SPR screening of CMBLs already revealed the binding affinity of few CMBL analogues (CMBL3a and 7b) towards telomere DNA repeat DNA that formed G-quadruplex indicating the potential of these molecules for regulation of telomere length and hence could be a potential candidate molecule for telomere targeted therapy. Towards this goal, second part (Part II) of my study involved to evaluate the regulatory effect of CMBL3a and 7b on cell cycle and cancer phenotypes and relative telomere length. Further elucidation underlines the molecular mechanism of regulation.

2. MATERIALS AND METHODOLOGY

2.1 Cell Culture

Materials

T-75 cell culture Flask, DMEM Powder, High Glucose (Gibco), Fetal Bovine Serum,(FBS, Gibco), 1X Phosphate Buffer Saline, NaCl 8gm, KCl 200mg, Na₂HPO₄ 1.44gm, KH₂PO₄ 240mg, 1X Trypsin EDTA (Gibco), 10ml Penicillin Streptomycin without glutamate (Pen Strep, Gibco) per litre of DMEM medium, Cell Line: **Ca Ski**, 3.6gms of Sodium bicarbonate (NaHCO₃) per litre of DMEM medium, 5.7gms of HEPES per litre of DMEM medium

Methodology

Take a flask of early passage of cell line and split at 80% confluent, remove the medium and give wash 1X PBS twice, add 2ml of 1X Trypsin-EDTA to the flask and incubate in CO₂ incubator (5-7 minutes), add 5ml of DMEM with 10% FBS, centrifuge at 1650rpm for 5 minutes at RT, discard supernatant and re-suspend the pellet with 5ml DMEM with 10% FBS, Count the cells using hemocytometer and seed back 1.5×10^6 to fresh T-75 flask, incubate in CO₂ incubator and allow to be 80% confluent till next passage.

Freezing of Cells (storing cell line): After trypsinizing the cells from 80% confluent flask, add 3ml of freezing medium.

Freezing of Cells

- After trypsinizing the cells from 80% confluent flask, add 3ml of freezing medium
- Freezing medium = 2800µl FBS + 150µl DMSO
- Add 1 ml of total solution to each freezing vial

2.2 Cytotoxicity assay

Materials

- Flat Bottom Cell Culture 96 well plates (FALCON)
- Cell proliferation reagent WST-1

- CaSki and HaCaT cell lines
- DMEM (Gibco)
- FBS (Gibco)
- CMBLs

Methodology

Seed $0.07 \times 10^6 / 0.06 \times 10^6$ cervical cancer cell line CaSki cells per well in 96 well plate in a final volume of 100ul/well DMEM containing 10% FBS. After 24 hours of incubation treat the cells with the required concentration of CMBL, creating experimental triplicates for each of the concentration. After the required incubation of the cells with drug, add 10% cell proliferation reagent WST-1 in DMEM containing 10% FBS making the final volume 100ul / well, incubate it for 1 hour. Shake the plate for 10 seconds before taking the reading. Take the reading of absorbance in Spectramax M5 at 450nm of wavelength. Measure the absorbance of the samples against the control sample.

Analysis and calculation

- Transfer the data in excel sheet. Take the average of the experimental triplicates and find out the percentage standard deviation.
- Normalize the values with respect to the untreated controls.
- Plot the graph on the Graphpad Prism8 version 8.0.2.

2.3 Scratch Wound Healing Assay

Materials

- Flat Bottom Cell Culture Plates 12-well (Corning Costar)
- DMEM, High Glucose (Gibco) containing 1% and 10% Fetal Bovine Serum (Gibco)
- Mitomycin-C (Fisher BioReagents)
- Fibronectin Human Protein, Plasma (Gibco)
- 1x Phosphate Buffer Saline (PBS)
- 200µl tip for scratch
- Bright field Microscope for visualizing (IX 73 Olympus Inverted Microscope)

- CellSens software for image capturing
- ImageJ software for analysis

Methodology

Plate 0.26×10^6 cells per ml per well in 12 well plate in DMEM culture medium with 10% FBS, allow the cells to grow for 7-8 hrs such that the wells get 90-95% confluent. Give two washes of 1x PBS, treat the cells with mytomycin- $2\mu\text{g}$ in per ml of DMEM containing 1% FBS, incubate for two hours, put a scratch with 200 μl tip, wash the wells with DMEM containing 1% FBS, add 1ml of DMEM containing 1% FBS per well, treat the scratched wells with required concentration of CMBLs. Take the images at 0hr and 9th hour using the bright field microscope., analyze the area closure using Fiji Image software. Each of the concentration was performed in experimental as well as biological triplicates

Calculation of percentage area covered

- Use imageJ to find out the area of the scratch at 0th hour say(x) of treatment and 9th hour say(y) of treatment the area. Use the free polygon tool to mark the scratch area and then use the measure tool to measure the area. Take the area value of 0th hour(x) and 9th hour(y).
- Put the x and y value in excel sheet to perform the further calculation.
- Subtract the area value of 9th hour from 0th hour say(x-y). Calculate the percentage area covered like this $(x-y/x*100)$.
- Take the average of the percentage area covered using the experimental triplicates say (z). Do the same for the control as well as treated samples.
- Set the control value as 100 by dividing the value by itself and multiplying it with 100.
- Normalize the treated values with respect to the control values
- Calculate the percentage standard deviation using the standard deviation function in excel sheet.
- Plot the graph on the Graphpad Prism8 version 8.0.2 and calculate the p value on Graphpad Prism8 using one-way ANNOVA.

Trouble-Shooting

- Cells get over-confluent by the time of putting scratch

Instead of putting the scratch after 24 hrs of drug treatment, the cells are treated along with the scratching of cells. Such condition will give on time effect of drug over cell migration.

- Uneven detachment of cells after putting scratch

When the scratch is placed, because of the poor adhesion capacity of CasKi cells, there is uneven detachment of cells. Thus, the plates used are 90-95% confluent to avoid cells detachment. In addition pre-warm the media and PBS at 37 degrees to avoid the cells detachment.

- Cell death observed while monitoring wound closure

Caski cell line is observed to be sensitive to high concentration of mytomycin-c to cause cell death. Serum starvation for a longer period of time (12-16) hours can be used to synchronize cells to same cell cycle phase but cannot be assured fully. Thus, a minimal concentration of mytomycin-c is required (2µg per ml per well) is useful for CasKi cells instead of a standard 8 µg per ml per well treatment.

2.4 Cell Cycle Analysis

Materials

- CaSki cell line
- 6 well plate (corning)
- DMEM, FBS, 1XPBS
- 1X TE, 100% Methanol
- Propidium Iodide (Sigma)
- RNase, TritonX- 100 (Sigma)

Methodology

Seed 0.15×10^6 cells per well in a 6 well plate in 1ml of DMEM containing DMEM, allow it to grow for 24 hours in the incubator at 37 degrees, starve the cells by adding DMEM containing no FBS for 24 hours, treat the cells with the required concentration of drug and incubate it for required time period, after the required incubation take out the media of each well in designated eppendorfs and wash the wells with 1X PBS twice and add 100ul of TE, allow to detach the cells by putting the plates in incubator for 5-7 minutes, add back the aspirated media from the eppendorfs to designated wells, homogenize the mixture, collect the cells in the designated eppendorfs, centrifuge it at 1650 rpm, degree, 5 minutes, discard the supernatant, redissolve the pellet in 400ul of chilled 1X PBS, centrifuge it at 1650rpm , 4degrees, 5minutes, discard the supernatant and add 70% chilled ethanol in distilled water for fixation and store it in -20 refrigerator.

At the time of running the samples in BD FACS Verse, take out the samples centrifuge it at 1650 rpm for 5 minutes at 4degrees, discard the supernatant, add 1000ul of chilled 1XPBS, re-suspend the pellet, centrifuge it at 1650 rpm, 4degrees, for 5 minutes, discard the supernatant, redissolve the pellet in 500ul of the dye solution, homogenize properly and boil it at 37 degrees for 15 minutes and filter using nylon filter to remove the clumps.

Dye solution: 50mg/ml PI, 2mg/ml RNaseA, 0.1% TritonX-100

Run it in BD FACS verse machine using BD FACS suite software

Analysis and calculation

- Use the Flowjo software and Dean-Jetfox method for the analysis.
- Collect the data on excel sheet for further calculation for each of the cell cycle phases. Calculate the average for the triplicate values.
- Use the control to normalize the treated samples.
- Calculate the percentage standard deviation using the standard deviation function in excel sheet.

- Plot the graph on the Graphpad Prism8 version 8.0.2 and calculate the p value on Graphpad Prism8 using one way ANNOVA.

Troubleshooting

- Use nylon mesh filter to avoid of cells clumping
- Use 1x PBS free without Ca^{+2} and Mg^{+2}
- Add dropwise 70% chilled ethanol to the cells to homogenize the fixation
- Heat the samples before running to avoid getting the false result from the double stranded RNA present in the sample.

2.5 Apoptosis Assay

- CaSki cell line
- 6 well plate (CORNING)
- BD Annexin V PE apoptosis kit,
- DMEM (Gibco)
- FBS(Gibco)
- 1X TE (Gibco)
- 1X PBS

Methodology

Seed 0.4×10^6 cells per well in a well plate in 1 ml of DMEM containing 10% FBS and 1% penstrap, after 24 hours treat the cells with required concentration of CMBL, after the required time period of incubation extract the cells by the following method

Aspirate the media form the wells in the designated eppendorfs, wash the wells with 1X PBS twice, add 100ul of TE per well, incubate it for 5-7 minutes, aftere the detachment of cell form the surface add the extracted media from the designated eppendorfs to designated wells, homogenize the mixture and add back to the designated eppendorfs, centrifuge it at 4 degree, 1650 rpm for minutes, discard the supernatant, resuspend the pellet in 1 ml of 1X PBS, centrifuge at 4 degree, 1650 rpm for minutes, add 1ml 1x BB buffer to each sample, aliquot 100ul of each sample into designated eppendorfs, for

each control aliquot for 100ul for making (1 unstained, 1 for 7AAD dye, 1 for PE dye, 1 for mix) for each treated sample aliquot 100ul for mix

Add 2ul of respective dyes in the respective tubes in the mix add both the dye 7AAD as well as PE, spin down the samples incubate on ice for 15 minutes, add 500ul of 1XBB buffer to each sample, run it in BD FACS Verse machine using BD FACS suite software, analyse the results in BD FACS suite software.

Analysis and calculation

- Use the BD FACS suite software for the colour compensation with respect to control.
- Collect the data on excel sheet for further calculation. Calculate the average for the triplicate values.
- Use the control to normalize the treated samples.
- Calculate the percentage standard deviation using the standard deviation function in excel sheet.
- Plot the graph on the Graphpad Prism8 version 8.0.2 and calculate the p value on Graphpad Prism8 using one way ANNOVA.

Troubleshooting

A lot cell death is observed in the control sample. To minimize that:

- Complete the experiment in 1 hour.
- Use color compensation instead of making control for each sample for each dye.
- Always keep the samples on ice

Cells are lost during washing

- To avoid this use 1.5ml eppendorf instead of 2ml eppendorf
- To avoid disturbing the pellet, leave a little supernatant at the bottom after each wash.

Unstained cells should always be included in the experimental set-up to monitor autofluorescence and to set the gates.

2.6 Clonogenic Assay

Materials

- 6 well plate (CORNING)
- CaSki cell line
- DMEM (Gibco)
- FBS (Gibco)
- 1XPBS
- 1X TE (Gibco)
- Glacial Acetic Acid (Fischer Scientific)
- Mehtanol (Fischer Scientific)
- Crystal Violet (Sigma)
- Ix73 Bright Field microscope

Methodology

Seed 1000 CaSki cells per well in 6 well plate in 1ml of DMEM containing 10% FBS, after 24 hours of incubation treat the cells using the desired concentration of CMBL, after another 24 hour aspirate the old media and add 4ml of fresh DMEM containing 10% FBS and 1% penstrap, allow the colonies to grow for 10 days inside the incubator. After the 10th day take out the plates and aspirate the media, wash using 1X PBS, add 2ml of fixing solution (Acetic acid: methanol) (1:7) (vol/vol) incubate it for 10 minutes. Aspirate the fixing solution and add 0.5% crystal violet solution, incubate it for 2 hours with some slow agitation. After 2 hours rinse the plates with water and allow it to dry. Count the colonies using ix73 bright field microscopy (only consider the colonies which have more than 50 cells).

Troubleshooting

To avoid the media evaporation

- Add 4ml of 1xPBS in the plate cavities to reduce the media evaporation.

To avoid the cell detachment

- At the time of treatment do not remove the media to reduce the cell detachment from the wells
- After 24 hours of drug treatment use sides of the wells to add the media to avoid the cell detachment.
- Disturbing the plates in incubator also leading to detachment of cells to avoid that seed one extra plate without any treatment for monitoring the colony growth

3. Results and Discussions:

Part I. Screening of CMBLs (21 analogues) using scratch wound healing cell migration assay

3.1 Screening of CMBLs (21 analogues) using scratch wound healing cell migration assay

CMBL library comprises 21 analogues with little variation is their linker A and linker B. General Structure of CMBL described in Figure 3.1.a. To investigate the effect of CMBL library of compounds on migratory phenotype, wound healing assay was performed using migratory cervical cancer cell line CaSki. Three concentrations (1 μ M, 2 μ M and 5 μ M) were used for the drug treatment and 9 hours incubation was done before taking the last image of the monolayer scratch. Bar graph for the percent wound closure obtained for 21 CMBL analogues in dose dependent manner depicted in (figure 3.1.b)

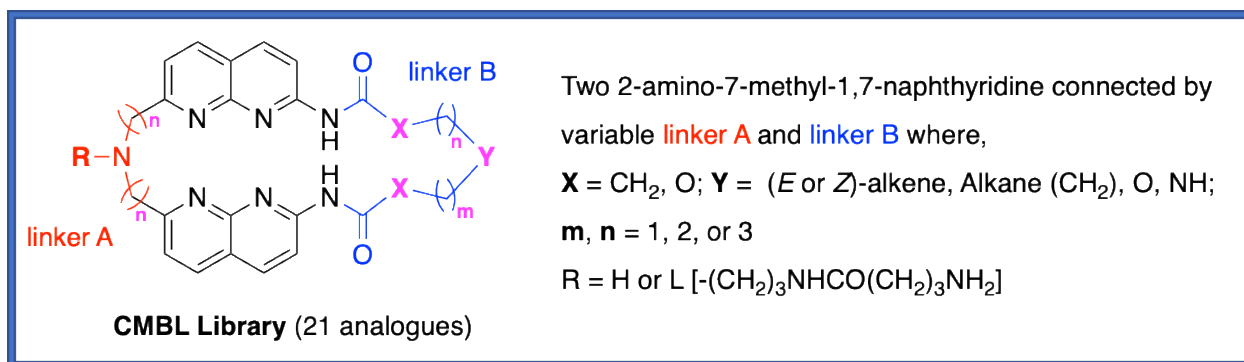


Figure 3.1.a General chemical structure of CMBL library

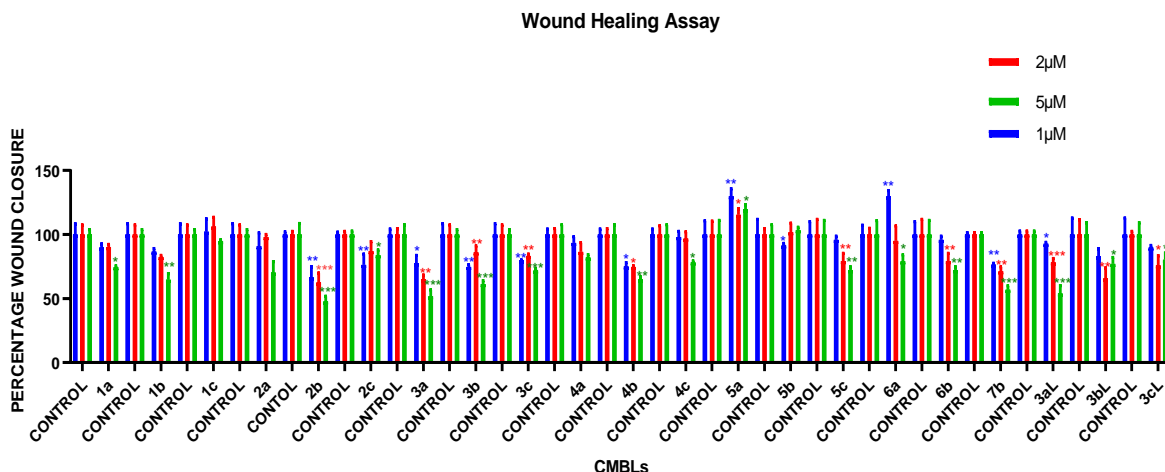


Figure 3.1.b Results of wound healing assay of 21 CMBL analogues

Figure 3.1.b Experimental result of wound healing scratch assays of 21 CMBL analogues using metastatic cervical cancer cell line CaSki. The cells were treated with mitomycin 2 hours prior making a monolayer scratch followed by treatment of CMBLs. Treatment was done with dose dependent manner using three concentrations of CMBLs [1µM (blue), 2µM (red), and 5µM (green)] creating experimental duplicates. In control group cells were treated with same concentration DMSO in case of DMSO soluble drug. (depicted in the figure 3.1.b). Bars represent mean \pm s.d.. Assays are representative of three independent experiments (N=3). $P > 0.05$ *, $P \leq 0.05$ **, $P \leq 0.01$ ***, $P \leq 0.001$ **** compared to control.

3.2 Categorization of CMBLs into three parts based on the cells ability to invade the empty spaces

The results in the figure3.1.b shows that the library of CMBL compounds can be categorized into three subparts based upon the cells ability to invade the empty spaces upon its treatment.

1. 1µM, 2µM, and 5µM treatment of CMBLs that inhibits the migration of cells shown in the figure below (figure 3.2.a-3.2.c)
2. 1µM, 2µM, and 5µM treatment of CMBLs that promotes the migration of cells (figure 3.2.d-3.2.f)
3. 1µM, 2µM, and 5µM treatment of CMBLs that does not have any significant effect on migration (figure 3.2.g-3.2.i)

Table 3.2.a Fold change of wound closer in the presence of CMBL analogues

CMBL	Fold change for wound closer after treatment of CMBL		
	1.0 μM	2.0 μM	5.0 μM
1a	0.90	0.90	0.74
1b	0.87	0.82	0.65
1c	1.02	1.06	0.95
2a	0.91	0.98	0.70
2b	0.66	0.63	0.48
2c	0.76	0.87	0.84
3a	0.78	0.65	0.52
3b	0.75	0.86	0.61
3c	0.80	0.83	0.72
4a	0.93	0.87	0.82
4b	0.75	0.75	0.65
4c	0.98	0.97	0.78
5a	1.30	1.15	1.20
5b	0.91	1.02	1.03
5c	0.96	0.79	0.72
6a	1.30	0.95	0.79
6b	0.96	0.79	0.72
7b	0.76	0.71	0.57
3aL	0.93	0.78	0.54
3bL	0.83	0.66	0.77
3cL	0.90	0.76	0.80

At lower concentration (1.0 μM) we observed nine CMBL analogues [2b (0.66) > 3b, 4b (0.75) > 7b, 2c (0.76) > 3a, 3aL (0.78) > 3c (0.80)] showed the significant inhibitory effect on CaSki cell migration with fold change ranging from 0.66 to 0.80 (Table 3.2.a). Among these eight compound 2b showed the maximum inhibitory effect (fold change 0.66). At this concentration (1 μM) two CMBL analogues 5a and 6a were observed to promote CaSki cell migration with 1.3-fold. Rest of the 11 analogues showed no significant effect on wound closing of CaSki cell. At two-time higher concentration (2.0 μM) we observed additionally five more CMBL (5c, 6b, 3aL, 3bL and 3cL) demonstrated significant inhibition on CaSki cell migration. At 2.0 μM , little acceleration in migration was observed in case of 2c (fold change 0.87) compare to 1 μM concertation. With further increase in the CMBL concentration to 5 μM we observed except four analogues (1c, 4a, 5b and 5a) all CMBLs exhibited inhibitory effect on CaSki cell migration with the fold change ranging from 0.48 to 0.84. At higher concentration (5 μM) 5a display 1.2-fold stimulation in the wound healing. Dose dependent wound healing data revealed 2b showed the highest inhibitory effect at all three concentrations [fold change 0.66 (1.0 μM), 0.63 (2.0 μM) and 0.48 (5.0 μM), in contrast 5a showed the consistently acceleration of the migration.

Overall, from these data we can categorized the CMBL into three categories as follow:

1. CMBL that inhibit the migration of CaSki cells (figure 3.2.a-3.2.c)

At 1 μM : 2b, 2c, 3a, 3b, 3c, 4b, 7b and 3aL

At 2 μM : 2b, 3a, 3b, 3c, 3aL, 4b, 5c, 6b, 7b, 3aL, 3bL, 3cL

At 5 μM : 1a, 1b, 2a, 2b, 2c, 3a, 3b, 3c, 4b, 4c, 5b, 5c, 6a, 6b, 3aL, 3bL, 3cL

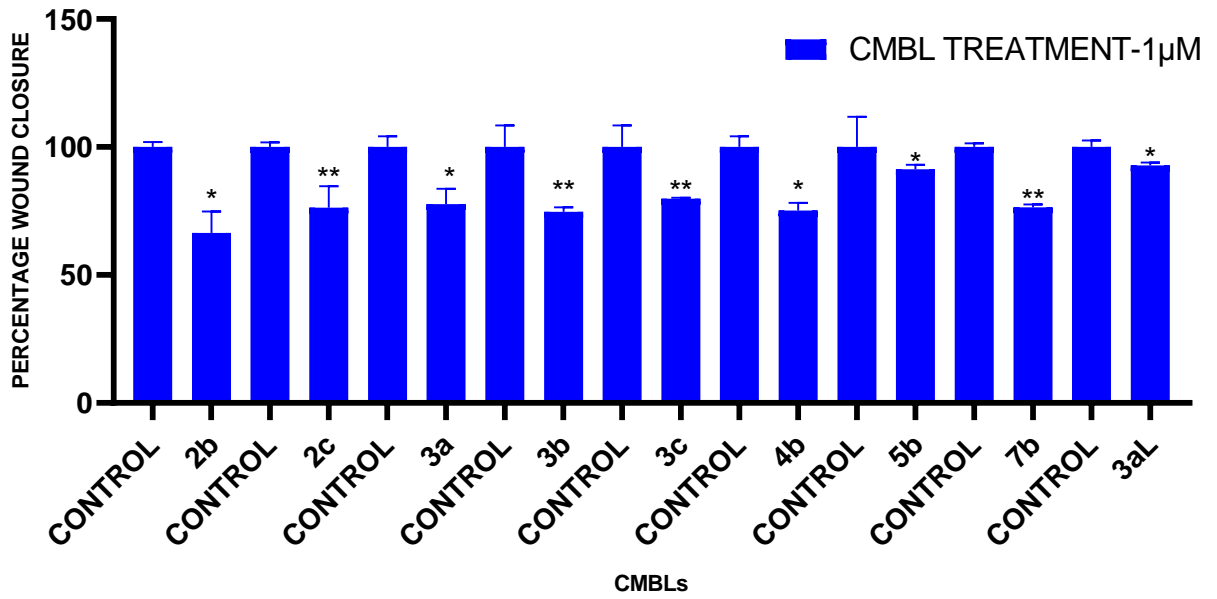


Figure 3.2.a CMBLs that are inhibiting migration in 1µM treatment

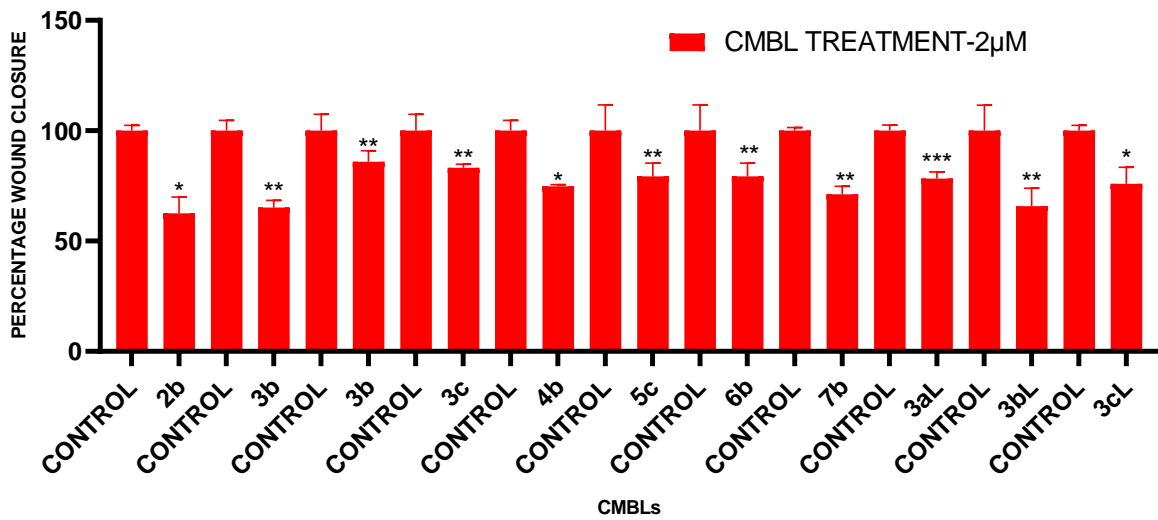


Figure 3.2.b CMBLs that are inhibiting migration in 2µM treatment

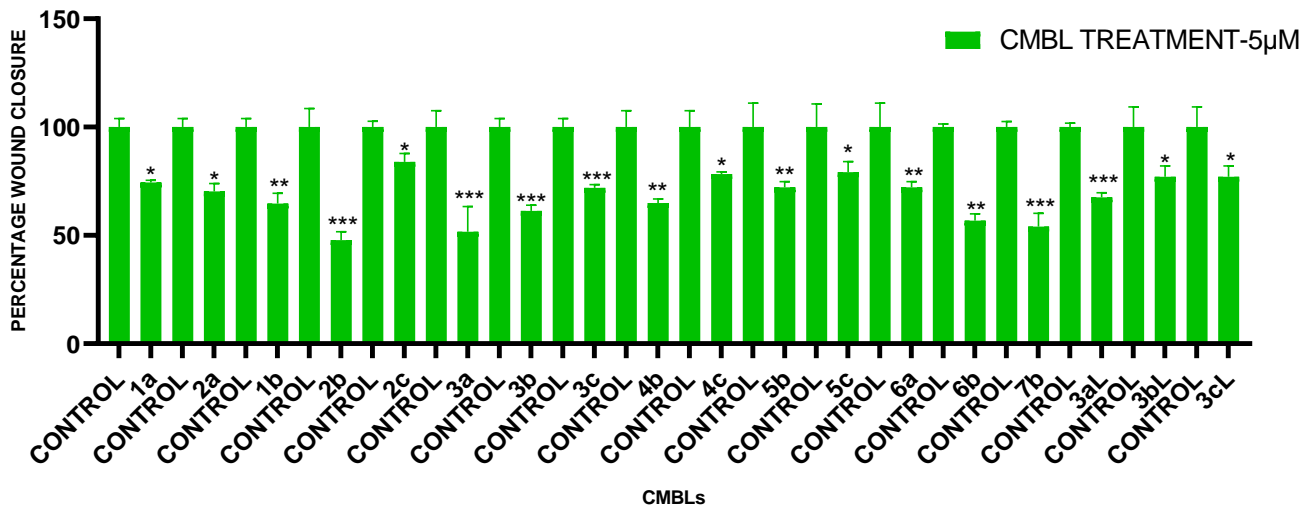


Figure 3.2.c CMBLs that are inhibiting migration in 5µM treatment

2. CMBLs that promote the migration of cells (figure 3.2.d-3.2.f)

At 1 µM: 6a, 5a

At 2 µM: 5a

At 5 µM: 5a

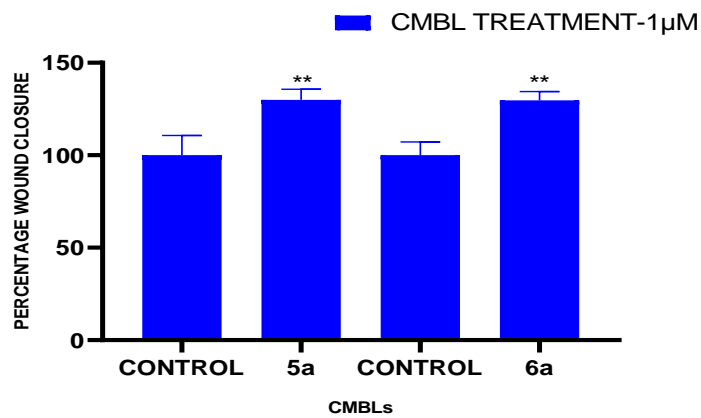


Figure 3.2.d CMBLs that are promoting migration in 1µM treatment

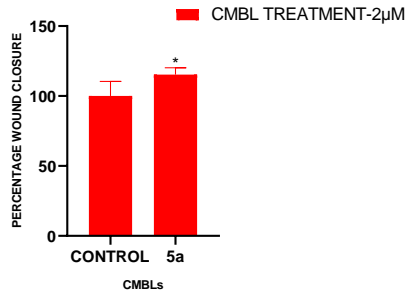


Figure 3.2.e CMBLs that are promoting migration in 2µM treatment

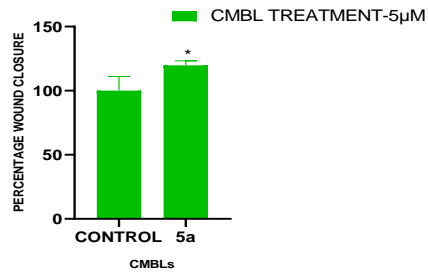


Figure 3.2.f CMBLs that are promoting migration in 5µM treatment

3. CMBLs that are not showing noteworthy effect (figure 3.2.g-3.2.i)

At 1 µM: 1a, 1b, 1c, 2a, 4a, 4c, 5b, 5c, 6b, 3bL, 3cL

At 2 µM: 1a, 1b, 1c, 2a, 2c, 4a, 4c, 5b, 6a

At 5 µM: 1c, 4a, 5b

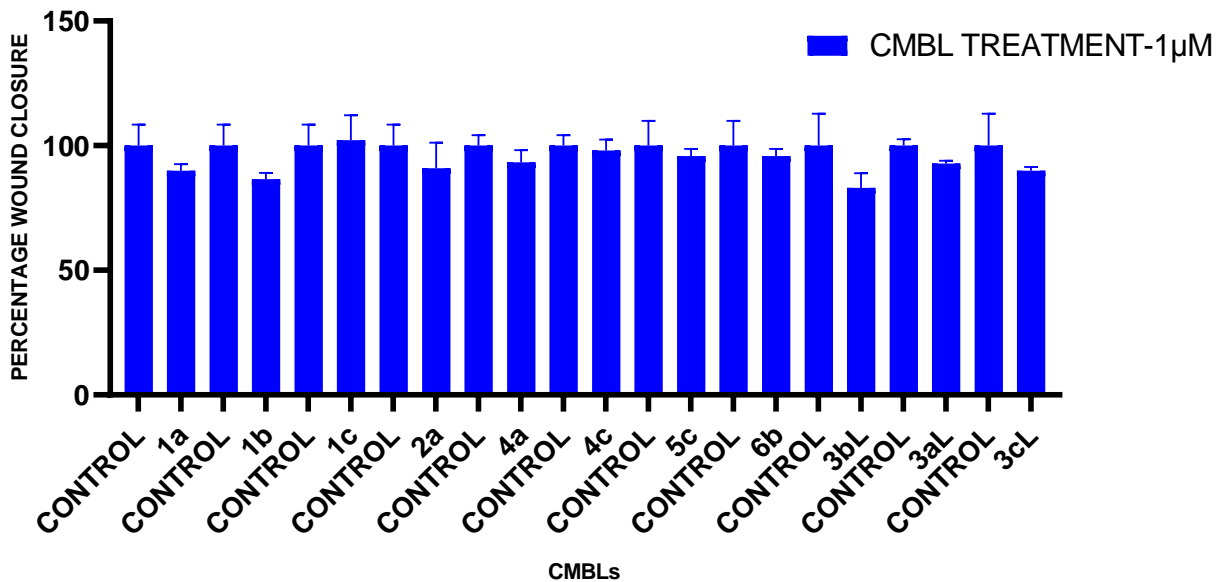


Figure 3.2.g CMBLs showing non-significant effect on migration (1µM treatment)

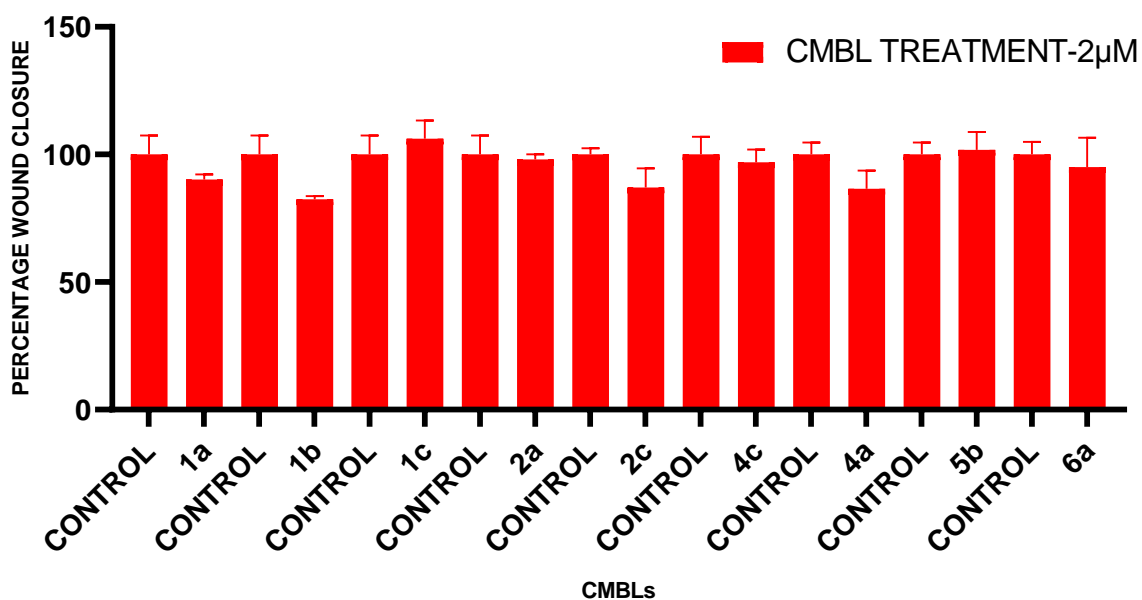


Figure 3.2.h CMBLs showing non-significant effect on migration (2µM treatment)

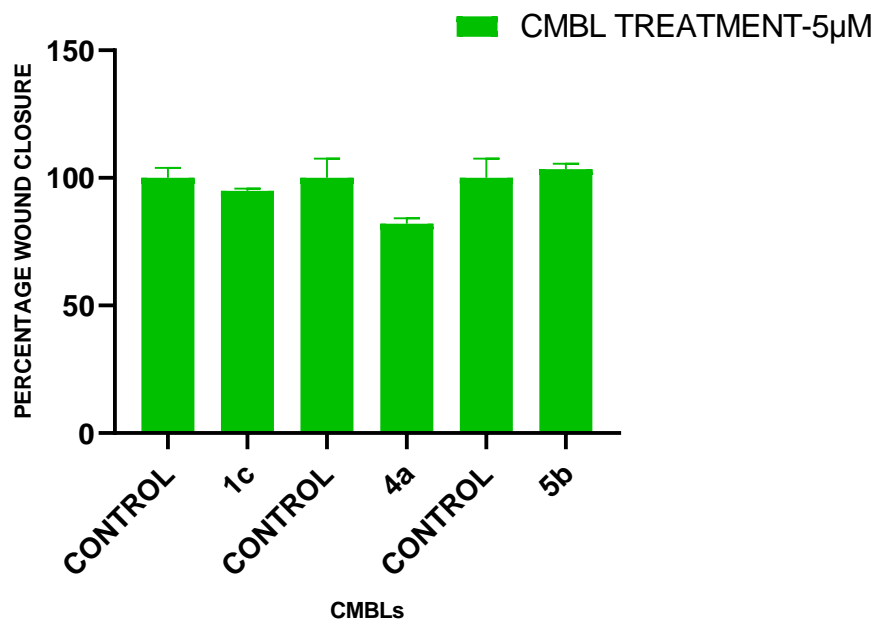


Figure 3.2.i CMBLs showing non-significant effect on migration (5µM treatment)

Slight variations in the chemical structure of these small molecules play a vital role in their functions. CMBL5a (Y = NH), 5b (Y = O), 5c (Y = CH₂), 6a (Y = *E*-alkene) and 6b (Y = *Z*-alkene) comprise 7 atoms between two carbonyl carbons in linker B with

single variation (Y) (depicted in figure 3.2.j general formula for CMBL) in their chemical structure. 5a which comprises one secondary amine group (NN) in linker B significantly accelerates the migration of CaSki cell at all three doses. On changing the NH group of 5a to bivalent oxygen 'O' in 5b, no significant effect on migration was observed. Whereas, changing the NH group to alkane (CH₂) (5c) or *E*-alkene (6a) or *Z*-alkene (6b) we observed significant inhibition at 5 μM concentration (Figure 3.2.k). These data clearly indicated the linker dependent tuning of the regulatory effect of CMBL on migratory phenotype. Previous reported studies of CMBL and its tuning binding affinity and selectivity towards biologically significant nucleic acid sequence clearly indicated the potential of CMBL as drug candidate. Even these data revealed combining phenotype data of CMBL with its gene target could lead to evaluate the potential of CMBL as anti-cancer drug candidate.

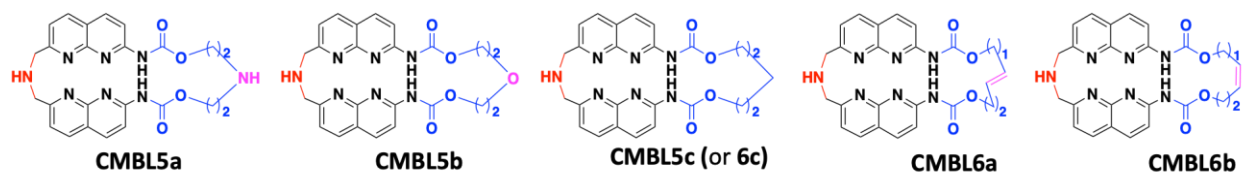


Figure 3.2.j Chemical structure of CMBL5a, 5b, 5c (or 6c), 6a and 6b comprise 7 atoms between two carbonyl carbons in linker B with single variation in Y (Figure 1.a in introduction general formula of CMBL).

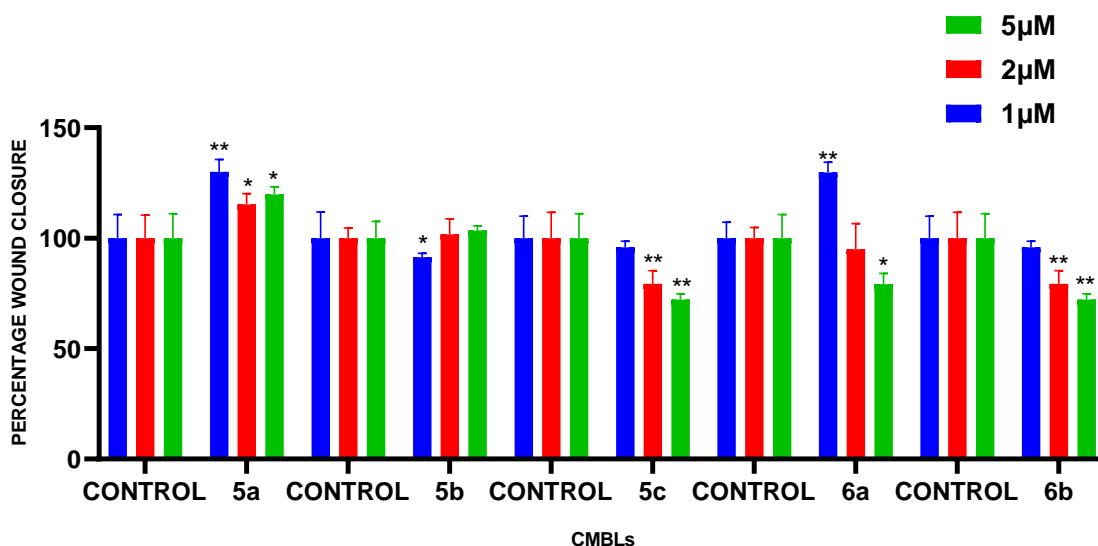


Figure 3.2.k showing change in the linker effects migration

Part II: Evaluation of regulatory role of telomere DNA binding CMBLs on cancer phenotype

As mentioned in the introduction SPR based screening of CMBL library already revealed the binding affinity of few CMBL analogues towards telomere repeat DNA. This part of my study focuses on the evaluation of the effect of two telomere repeat DNA binding CMBL analogues (CMBL3a and 7b) on cervical cancer phenotypes, relative telomere length. Further elucidation will underline regulatory molecular mechanism.

3.3 CMBL7b and CMBL3a is cytotoxic for human cervical cancer cell line CaSki with little effect on Normal Human keratinocytes HaCaT

Towards this goal we first performed cell viability assay cell proliferation reagent WST-1. Cytotoxicity was evaluated using cervical cancer cell lines (CaSki) and non-tumorigenic immortal keratinocyte cell lines (HaCaT) in the presence of CMBL3a and 7b. Among the two compounds investigated, CMBL3a as well as CMBL7b both showed the decreased viability of cervical cancer cell line CaSki in a concentration and time dependent manner with IC₅₀ values of 12.75 μ M for 24 hours 4.27 μ M for 48 hours and 2.27 μ M for 72 hours in CaSki for CMBL7b (figure a). Similarly, CMBL3a has IC₅₀ value of 16.9 μ M for 24 hours, 14.8 μ M for 48 hours and, 6.4 μ M for 72 hours (figure c). Furthermore, CMBL7b and 3a toxicity was checked in the normal human keratinocytes cell HaCaT. Results obtained so far are quite promising (figure c-d). Notably, CMBL7b and CMBL3a appeared to have a small effect on the viability shown in the table 2.1. These data suggested a relative selectivity of the drug for cancer cells.

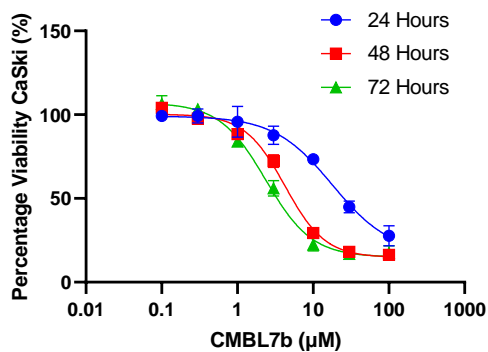


Figure a

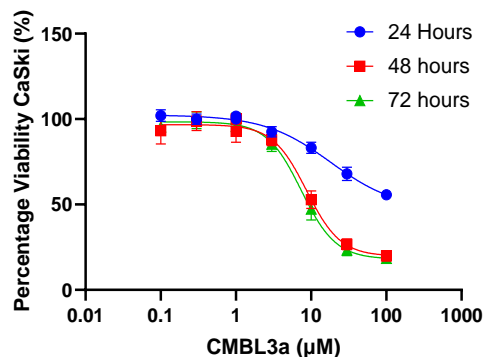


Figure b

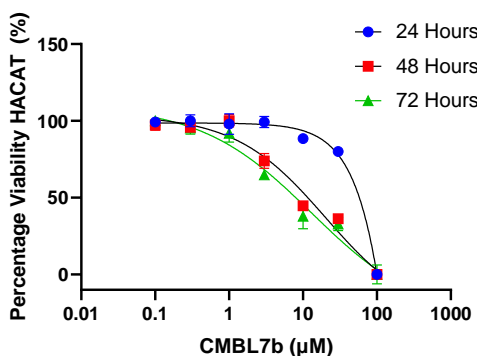


Figure c

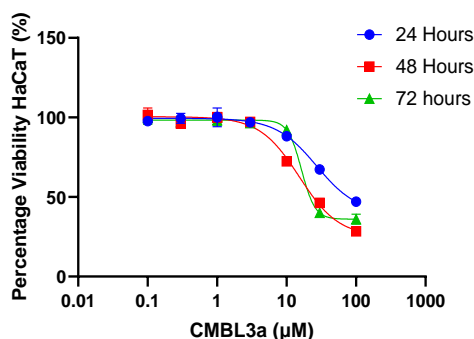


Figure d

Figure 3.3 CMBL7b and CMBL3a is cytotoxic for human cervical cancer cell line CaSki with little effect on Normal Human keratinocytes HaCaT. The growth inhibition effects were determined by WST colometric assay and the IC₅₀ was calculated by GraphPad Prism 8.0.2 software through a nonlinear fit curve (log of compound concentration versus normalized response-variable slope). (a-b) represents the cytotoxic analysis done on cervical cancer cell line CaSki with CMBL7b and CMBL3a at time and dose dependent manner respectively. (c-d) represents the cytotoxic analysis done on human keratinocyte cell line HaCaT with CMBL7b and CMBL3a at time and dose dependent manner respectively. Each point in the graph represent mean±s.d. Assays are representative of at least three independent experiments n=3. **P<0.01, *P<0.05 compared with untreated control

Table 3.3.a showing the IC₅₀ values of CMBL7b and CMBL3a on CaSki and HaCaT cell line, with their respective standard deviation value in the brackets.

IC ₅₀ values (µM)	24 hours	48 hours	72 hours
CaSki treated with CMBL7b	12.75 (0.1)	4.27 (0.28)	2.27 (0.28)
HaCaT treated with CMBL7b	39.83 (2.5)	10.17 (1.8)	7.24 (1.1)
CaSki treated with CMBL3a	16.17 (0.10)	14.8 (2.1)	6.4 (1.5)
HaCaT treated with CMBL3a	26.19 (2.6)	15.19 (1.8)	16.42 1.1)

3.3 Dose dependent treatment of CMBL7b in cervical cell line CaSki induces apoptosis

Having observed cytotoxicity of CMBL7b in the CaSki cervical cancer cell line compared to normal human keratinocyte epithelial cell line (HaCaT), we assayed CaSki cells for apoptosis induction on drug treatment in a dosage and time-dependent manner. The cells were cultured in DMEM (+10% FBS) for 24 hours, following which CMBL7b treatment (0.25 mM to 5 mM) was given for 24 and 48 hours. Apoptosis and cell death were respectively assayed for by phycoerythrin (PE)-conjugated Annexin V and 7-Aminoactinomycin D (7-AAD) co-staining of treated CaSki cells, followed by flow cytometric analysis; the 7-AAD dye is excluded by viable cells, while Annexin V-PE marks apoptotic cells. Cells analyzed by flow cytometry were categorized into four populations: the Annexin V⁺/7-AAD⁻ and Annexin V⁺/7-AAD⁺ quadrants were classified as early and late apoptotic cells, respectively, while the Annexin V⁻/7-AAD⁻ and Annexin V⁻/7-AAD⁺ quadrants were classified as living cells and necrotic cells, respectively. The results reveal that CMBL7b induces apoptosis in CaSki cervical cancer cells, as evidenced from Figure 3.4.m-n, with the treated cells showing an increase in apoptosis in a concentration and time-dependent manner. Furthermore, the results revealed that the apoptotic cell population was significantly increased by 24% at 24 hours post treatment and 54% at 48 hours post treatment, for a CMBL7b concentration of 5 μ M (figure 3.4.m-n).

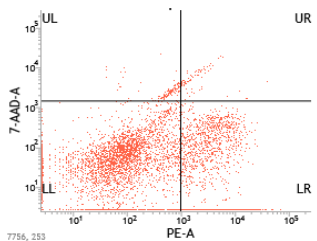


Figure a

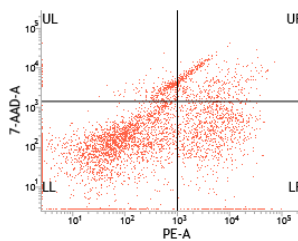


Figure b

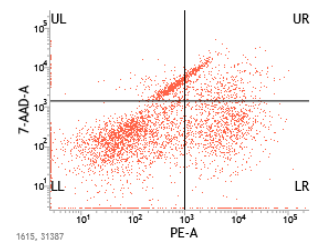


Figure c

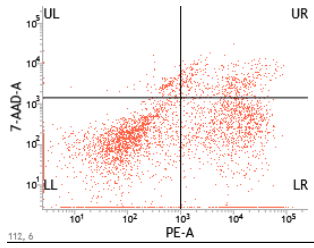


Figure d

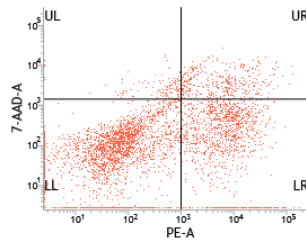


Figure e

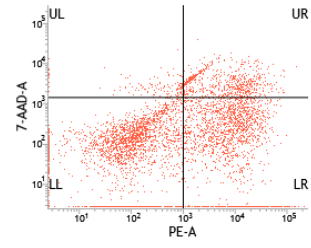


Figure f

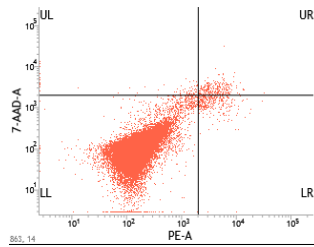


Figure g

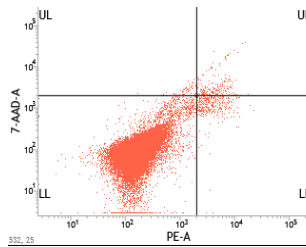


Figure h

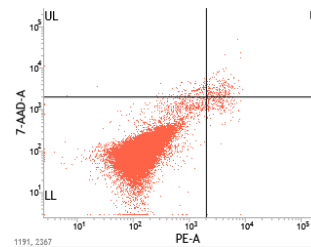


Figure i

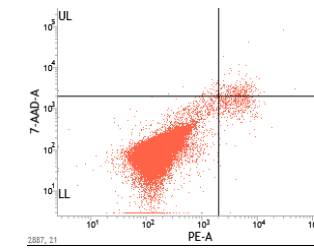


Figure j

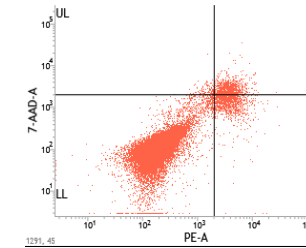


Figure k

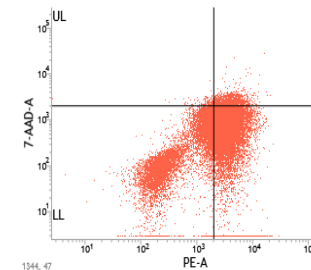


Figure l

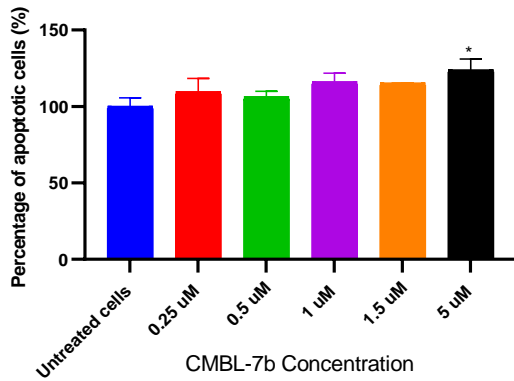


Figure 3.4.m CMBL7b 24 hours post treatment

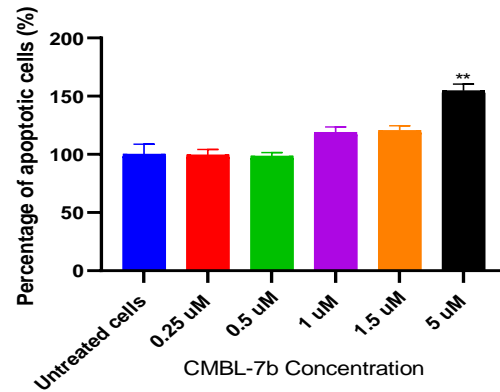


Figure3.4.n CMBL7b 48 hours post treatment

Figure 3.4 Treatment of CaSki cells with CMBL7b induces apoptosis in a dose-dependent manner. CaSki cells were incubated with different concentrations of CMBL7b for 24 and 48 hours, harvested and co-stained for Annexin V-PE and 7-AAD, followed by flow cytometry. (a-l) Scatter plots of cells treated with 0 μ M, 0.25 μ M, 0.5 μ M, 1 μ M, 1.5 μ M and 5 μ M CMBL7b, in order, for (a-f) 24 hours and (g-l) 48 hours. In each plot, the four quadrants represent the cell characteristic; viable cells are Annexin V and 7-AAD double-negative in the lower left (LL) quadrant, cells in late apoptosis or dead are both Annexin V and 7-AAD positive in the upper right (UR) quadrant, and cells in early apoptosis are Annexin V positive and 7-AAD negative in the lower right (LR) quadrant. (Figure3.4.m-n) The bar graphs represents the percentage of both late and early apoptotic cells at 24 and 48 hours post treatment, respectively, calculated based on flow cytometry, color compensation analysis and normalized to their respective controls. Bars represent mean \pm s.d. Assays are representative of three independent experiments (N=3). **P<0.01, *P<0.05 compared to the untreated control.

3.5 CMBL3a (7 μ M) induces apoptosis post 24 hours treatment in cervical cancer cell line CaSki

In order to determine if CMBL3a can also induce apoptosis in CaSki cells, a similar flow cytometric approach was employed to establish a dosage and time dependence. The results revealed that the percentage of apoptotic cells are significantly increased only at a drug concentration of 7 μ M, 24 hours post treatment (figure 3.5.i-j), but not 48 hours post treatment, suggesting that CMBL3a induces apoptosis at a specific time and dosage.

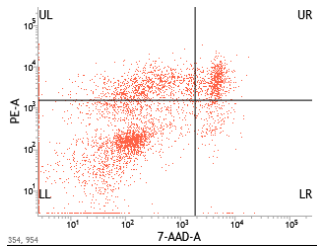


Figure a

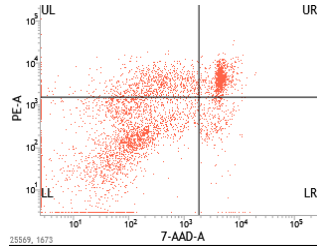


Figure b

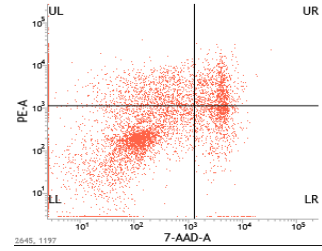


Figure c

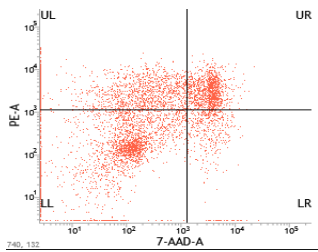


Figure d

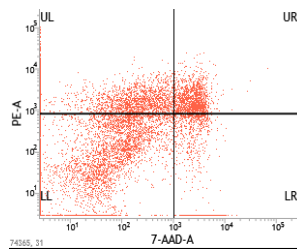


Figure e

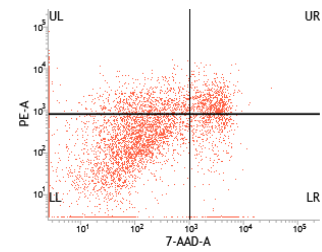


Figure f

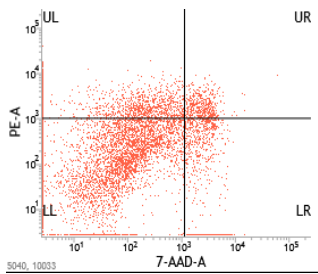


Figure g

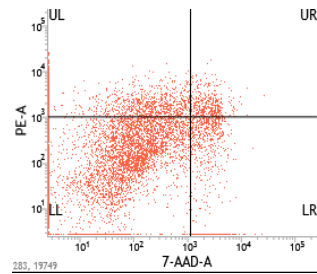


Figure h

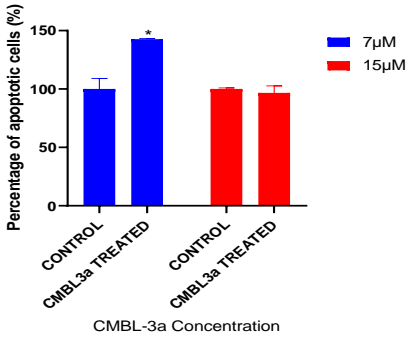


Figure 3.5.i CMBL3a 24hours post treatment

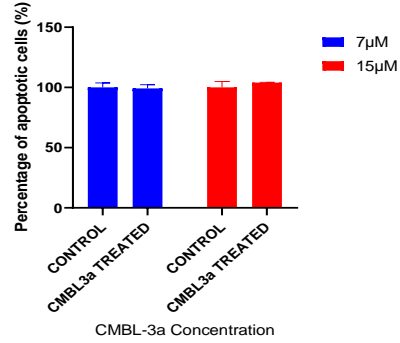


Figure3.5.j CMBL3a 48hours post treatment

Figure3.5. CMBL3a (7 µM) induces apoptosis post 24 hours treatment in cervical cancer cell line CaSki. (a-h) shows dose dependent and time dependent response of CMBL3a (7 µM & 15 µM) on cervical cancer cell line CaSki through apoptosis assay. CaSki cells were incubated for 24 and 48 hours at (7 µM & 15 µM) treatments. Cells were harvested and labeled with Annexin V- PE in conjugation with 7-AAD, cell apoptosis was determined by flow cytometry. Scatter plots of cells treated with CMBL3a (7µM and 15µM) with their respective concentration of DMSO control, in order, (a and g) represents response of DMSO treated in the same concentration as in 7 µM drug post for 24 hours and 48 hours treatments respectively. (b and f) represents response of cells treated with CMBL3a (7 µM) post 24 hours and 48 hours treatments respectively. (c and g) represents the DMSO treated control (same concentration as in CMBL3a) post 24 hours and 48 hours treatment respectively and (d and h) represent response of CMBL3a (15µM) post 24 hours and 48 hours treatment respectively. In figure (a-h) the four quadrants represent the cell characteristic, viable cells are PE Annexin and 7-AAD negative in the third quadrant named Lower left (LL), cells in late apoptosis or dead are both PE Annexin and 7-AAD positive in second quadrant named Upper right (UR), cells in early apoptosis phase are PE Annexin V positive and 7-AAD negative present in the first quadrant named upper left (UL). (Figure 3.5.i-3.5.j) represents the percentage of late apoptotic and early apoptotic, calculated based on flow cytometry color compensation analysis. Bars represent mean±s.d. Assays are representative of at least three independent experiments n=3. *P<0.05 compared with DMSO control.

3.6 CMBL7b induces cell cycle arrest in G₂/M phase in cervical cancer cell line CaSki

Cell cycle analysis was performed towards understanding the molecular mechanism of CMBL7b cytotoxicity in CaSki cells. This analysis revealed a significant concentration-dependent accumulation of cells in the S phase 24 hours post drug treatment as compared to the control and, in contrast, a significant decrease in the number of cells in the G₀/G₁ and G₂/M phases by 24 hours at a drug concentration of 1.5 μ M (figure3.6.m) Also, CMBL7b induced a significant reduction of cells in the S phase as well as in G₀/G₁ phase of the cell cycle 48 hours post treatment that accounted for a reduction in S phase cells by 43% in a dose-dependent manner (figure3.6.m). Detailed analysis of the cell cycle distribution of CMBL7b revealed that 1.5 μ M CMBL7b triggered a significant increase in the proportion of cells accumulated at the G₂/M phase within 48 hours, indicating that CMBL7b may inhibit the G₂/M transition (figure3.6.m).

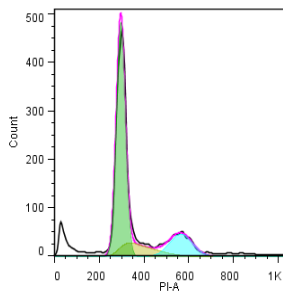


Figure a

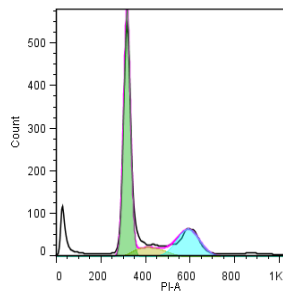


Figure b

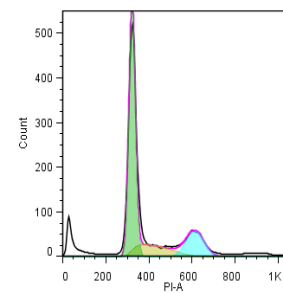


Figure c

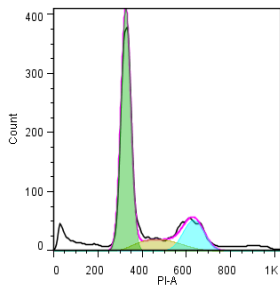


Figure d

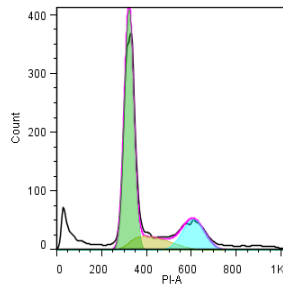


Figure e

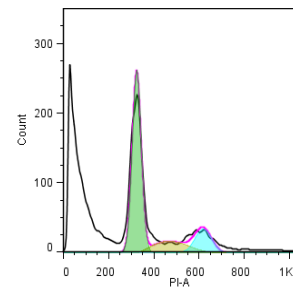


Figure f

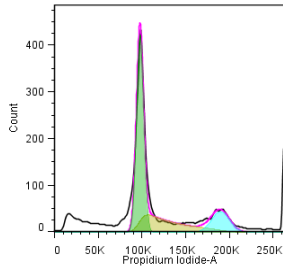


Figure g

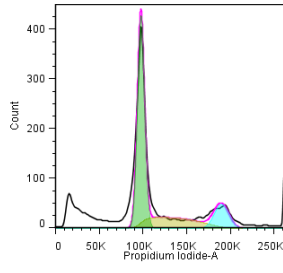


Figure h

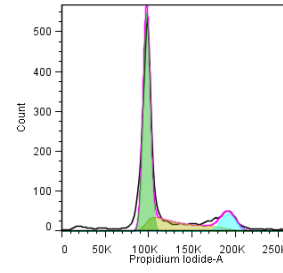


Figure i

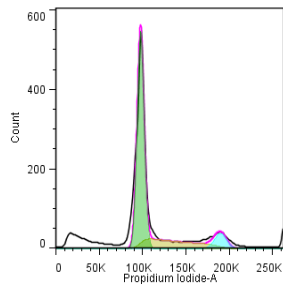


Figure j

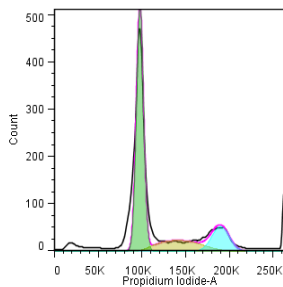


Figure k

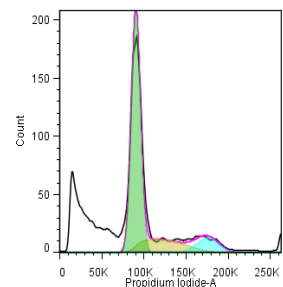


Figure l

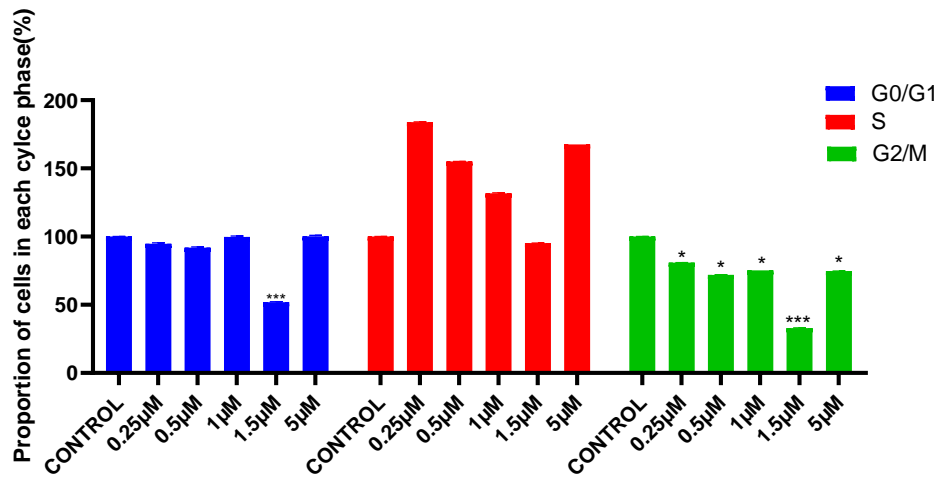


Figure 3.6.m CMBL7b dose dependent response on cell cycle analysis (post 24 hours)

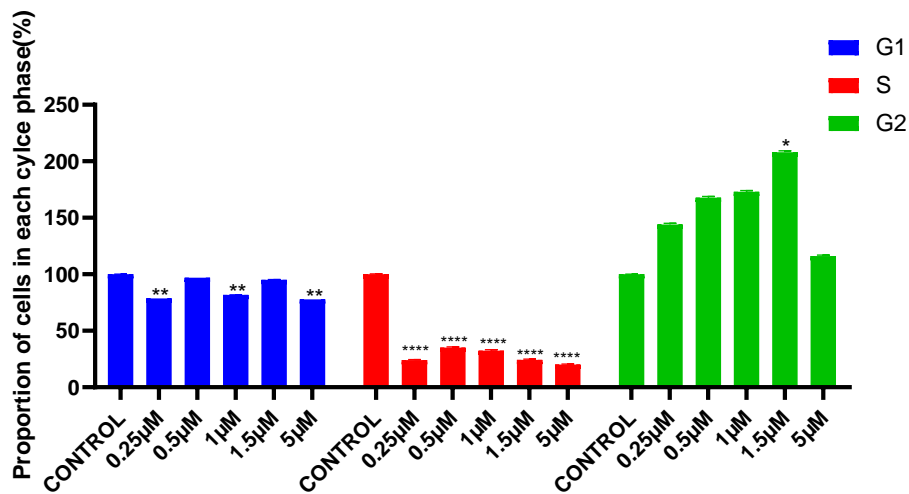


Figure 3.6.n CMBL7b dose dependent response on cell cycle analysis (post 48 hours)

Fig. 3.6 CMBL7b induces cell cycle arrest in CaSki cells. CaSki cells were incubated with different concentrations of CMBL7b for 24 and 48 hours, harvested and stained with PI, followed by DNA content analysis. (a-l) DNA histogram of cells treated with 0 μM, 0.25 μM, 0.5 μM, 1 μM, 1.5 μM and 5 μM CMBL7b, in order, for (a-f) 24 hours and (g-l) 48 hours. (Figure 3.6.m-n) represents the percentage of cells in each phase of the cell cycle at 24 and 48 hours, respectively. Bars represent mean \pm s.d. Assays are representative of three independent experiments (N=3). $P > 0.05$ *, $P \leq 0.05$ **, $P \leq 0.01$ ***, $P \leq 0.001$ **** compared to untreated control.

3.7 CMBL3a induces cell cycle arrest in S phase in cervical cancer cell line CaSki

In order to determine if CMBL3a can also induce cell cycle arrest in CaSki cells, a similar DNA staining approach was employed to establish time dependence treatment of CMBL3a. The results revealed that cells treated with 15 μM of CMBL3a for 24 and 48 hours exhibit a significant accumulation of cells in the S phase (164% and 80%, respectively) as compared to the control (Figure 3.7.e-f). Also, CMBL3a induced a reduction of cells in the G_0/G_1 phase of the cell cycle that accounted for a 15% reduction of G_0/G_1 phase cells post 24 and 48 hours of treatment (figure 3.7.e-f). Detailed analysis of the cell cycle distribution revealed that within 48 hours CMBL3a triggered an increase in the accumulation of cells in the G_2/M phase by 12% at 24 hours post treatment and decrease by 8% at 48 hours post treatment (figure 3.7.e-f). This indicates a possibly

irregular DNA replication and a resultant arrest of cell division in S phase due to the cytostatic effect caused by the drug, suggesting CMBL3a strongly inhibits cell division at the S phase.

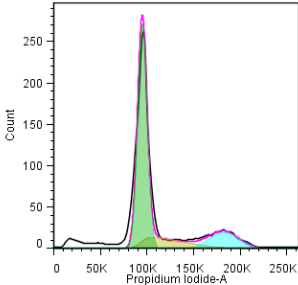


Figure a

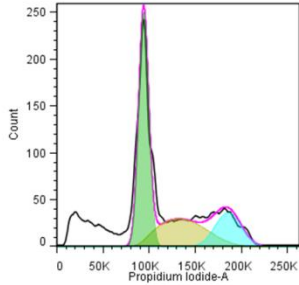


Figure b

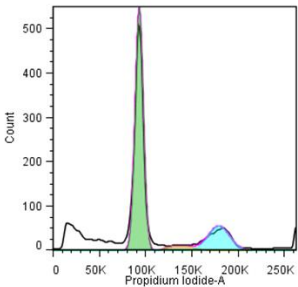


Figure c

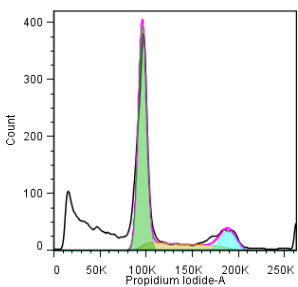


Figure d

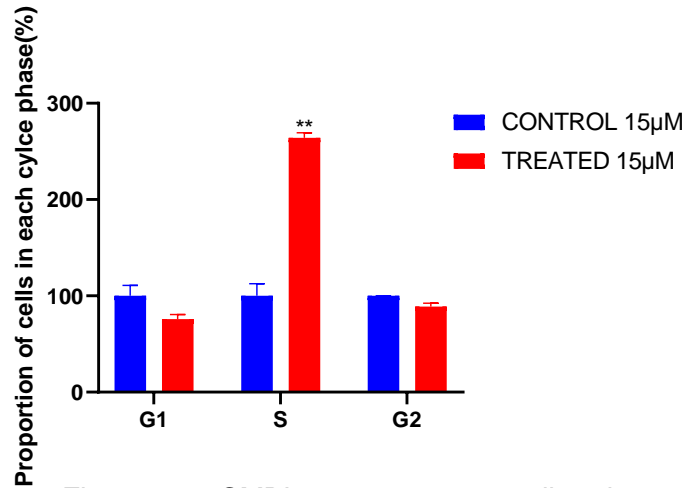


Figure 3.7e CMBL3a response on cell cycle analysis (post 24 hours)

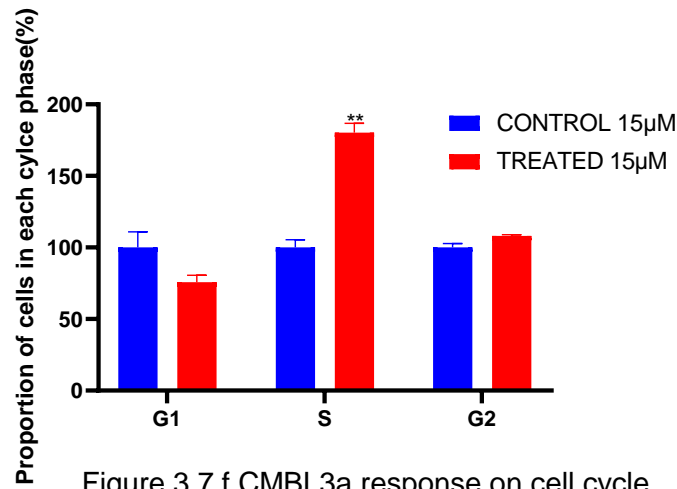


Figure 3.7.f CMBL3a response on cell cycle analysis (post 24 hours)

Figure 3.7 represents the effect of CMBL3a on cell cycle analysis. CaSki cells were incubated with a concentration of 15µM of CMBL3a for 24 and 48 hours, harvested and stained with PI, followed by DNA content analysis. DNA histogram of cells treated with 15µM of CMBL3a, in order, for (a and c) shows the results for DMSO treated controls (same concentration as in drug) post 24hours and 48 hours respectively. (c and d) represents the effect of CMBL3a (15µM) post 24hours and 48 hours respectively. (Figure 3.7.e-f) represents the percentage of cells in each phase of the cell cycle after treatment of CMBL3a in time dependent manner, post 24 hours and 48 hours respectively. Bars represent mean±s.d. Assays are representative of at least three independent experiments n=3. **P<0.01, *P<0.05 compared to DMSO control.

3.8 Clonogenic growth inhibition by CMBL7b and CMBL3a

Next we have used colony formation assay as a method of choice to determine cell reproductive death and its ability to form colonies after treatment with CMBLs. Different concentration of CMBL3a (7 μM , 15 μM) and CMBL7b (0.25 μM , 0.5 μM , 0.75 μM , 1 μM , 1.25 μM , 2 μM) was used for the treatment in a dose dependent manner for 24 hours. It was seen that only a fraction of the seeded cells retains the capacity to produce colonies. As can be seen in the (figure3.8.l-m) on increasing the concentration of CMBL7b and CMBL3a the ability to form colonies is reduced significantly from (100% to 8%) and (100% to 4%) respectively. Evidently from the results we can conclude that the CMBLs treatment is leading to reduction in the ability of the CaSki cell in a population to undergo unlimited division. Furthermore, we can conclude that the malignant potential of individual cell is getting reduced significantly and it is a potential indicative of the therapeutic efficacy of CMBL7b and CMBL3a.



Figure a
Control

Figure b
CMBL7b 0.25

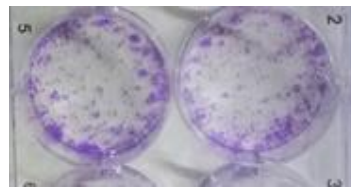


Figure c
CMBL7b 0.5 μM

Figure d
CMBL7b 0.75



Figure e
CMBL7b 1 μM

Figure f
CMBL7b 1.25



Figure g
CMBL7b 1.5 μM

Figure h
CMBL7b 2 μM

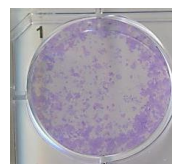


Figure i
DMSO Control

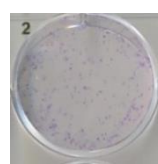


Figure j
CMBL 3a 7.5 μM

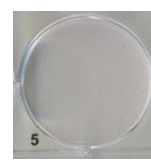


Figure k
CMBL 3a 15 μM

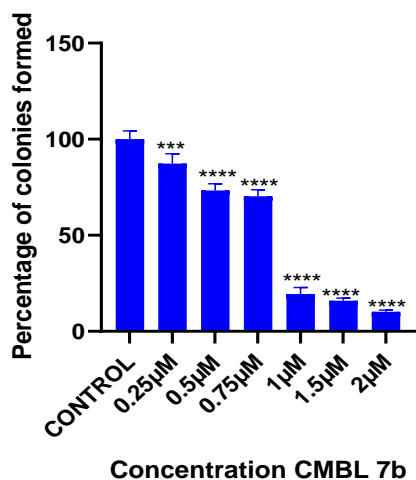


Figure 3.8.l Effect of CMBL7b on colony formation

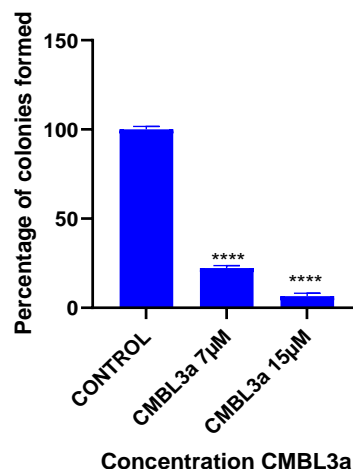


Figure 3.8.m Effect of CMBL3a on colony formation

Figure 3.8 Clonogenic growth inhibition by CMBL7b and CMBL3a. Cervical cancer cell line CaSki cells were treated with different concentrations of CMBL7b and CMBL3a for 24 hours using concentration (0.25 µM, 0.5 µM, 0.75 µM, 1 µM, 1.25 µM, 1.5 µM, 2 µM) and (7 µM, 15 µM) respectively. The cells were allowed to grow to form colonies for 10 days. At the 10th day the colonies were fixed using (1:7) ratio of acetic acid and methanol and were stained using 0.5% crystal violet. Counting of the colonies was done using the bright field microscope. (a-h) represents the effect of dose dependent response of CML7b on colony formation, as seen in the (figure 3.6.l) the ability to form colonies is decreased from (100%-8%) as the concentration of drug treatment is increased (0.25 µM, 0.5 µM, 0.75 µM, 1 µM, 1.25 µM, 2 µM). In the (i-k) represents the effect of dose dependent response of CML3a on colony formation, as seen in the (figure 3.8.m) the ability to form colonies is decreased from (100%-4%) as the concentration of drug treatment is increased (7µM, 15µM). Bars represent mean±s.d. Assays are representative of at least three independent experiments n=3. Assays are representative of three independent experiments (N=3). P > 0.05 *, P ≤ 0.05 **, P ≤ 0.01 ***, P ≤ 0.001 **** compared to control.

Conclusion: Result obtained from first part that is screening of 21 CMBL analogues using scratch wound healing migration assay revealed the linker dependent tuning of regulatory behaviour of CMBL towards cell migration. This data indicated sophisticated modification of linkers in CMBL chemical structure would have potential to switch the modulatory effect of CMBL as inhibitor or promoter or neutral towards cell migration. This data also identified few CMBL analogues comprising anti-migratory effect that would be a potential candidate for the treatment of metastatic cancer progression. Second part of this study focused on two CMBL analogues (3a and 7b) that have binding affinity for telomere DNA repeat. Result obtained from phenotypic assay revealed both

the compound have lower cytotoxicity towards normal human keratinocytes cell HaCaT compare to tumorigenic cervical cancer cell lines CaSki indicating tumor specific physiological activity of these compounds indicating that they could be potential candidates in targeting tumors with minimal side effects on normal cells. CMBL7b showed to have a significant effect on apoptosis as well as it evidently arrests the G₂/M transition by 24 and 48 hours treatment. By 48 hours post treatment, it causes a considerable reduction in the number of cells with replicated DNA preventing the cells from gearing up for mitosis. CMBL3a act as a strong inhibitor of cell division acting efficiently in the S phase of cell division but there was not any significant on apoptosis. Further from the clonogenic assays done with CMBL7b and CMBL3a it is evident that both the drugs are very efficient in inhibiting the unlimited cell proliferation of cervical cancer cell line CaSki. These findings suggest different modes of action for these two compounds in suppressing tumor cell growth indicating an intriguing possibility of multiple putative targets for efficiently treating tumor cell proliferation and metastases.

Future Perspectives:

- Validation of telomere shortening upon the CMBL3a and CMBL7b treatment on cervical cancer cell line CaSki, using the relative telomere length measuring kit.
- To understand the underline molecular mechanism of the anticancer effect of CMBL3a and CMBL7b, we need to carry out western blotting to check time and dose dependent change in the protein expression of different EMT markers, apoptosis markers as well different cell cycle associated proteins.

References:

1. Arbyn M, Weiderpass E, Bruni L, de Sanjosé S, Saraiya M, Ferlay J, Bray F. (2018). Estimates of incidence and mortality of cervical cancer in 2018: a worldwide analysis. *Lancet Glob Health* 8,e191-e203
2. Bartkova J, Horejsi Z, Koed K, Kramer A, Tort F, Zieger K, et al., (2005). DNA damage response acts as a candidate anti-cancer barrier in early human tumorigenesis. *Nature*. 434: 864–870
3. Behzad Mansoori, Siamak Sandoghchian Shotorbani, and Behzad Baradaran. (2014). RNA Interference and its Role in Cancer Therapy. *Adv Pharm Bull*. 4, 313
4. Chiara Mondello and A. Ivana Scovass. (2004). Telomeres, telomerase, and apoptosis. *Biochemistry and Cell Biology*. 2004, 82, 498
5. D. C. Swinney.(2013). Phenotypic vs. Target-Based Drug Discovery for First-in-Class Medicine. *Clin. Pharmacol. Ther.* 93, 299
6. David C. Swinney and Jason Anthony. (2011). How were new medicines discovered?. *Nat. Rev. Drug Discov* 10, 507
7. Daniel Gandia. (2019). The Phenotype Landscape of Cancer in the Genotype Era. *Cancer Studies and Molecular MEDICINE* 5, 26
8. d'Adda di Fagagna F, Reaper PM, Clay-Farrace L, Fiegler H, Carr P, Von Zglinicki T, et al., (2003). A DNA damage checkpoint response in telomere-initiated senescence. *Nature*. 426: 194–198
9. Glenn E. Croston. (2017). The utility of target-based discovery; *Expert Opinion on Drug Discovery* 12, 427
10. Hee-Sheung Lee, Mar Carmena, Mikhail Liskovykh, Emma Peat, Jung-Hyun Kim, Mitsuo Oshimura, Hiroshi Masumoto, Marie-Paule Teulade-Fichou, Yves Pommier, William C. Earnshaw, Vladimir Larionov and Natalay Kouprina. (2018). Systematic Analysis of Compounds Specifically Targeting Telomeres and Telomerase for Clinical Implications in Cancer Therapy. *Cancer Res.* 78, 6282
11. Islam MK, Jackson PJ, Rahman KM, Thurston DE. (2016). Recent advances in targeting the telomeric G-quadruplex DNA sequence with small molecules as a strategy for anticancer therapies. *Future Med Chem.* 8, 1259
12. Jerry W. Shay. (2016). Role of Telomeres and Telomerase in Aging and Cancer. *Cancer Discovery* 584
13. Joelle Roche. (2018). The Epithelial-to-Mesenchymal Transition in Cancer. *Cancer.* 10, 52
14. John G. Moffat, Joachim Rudolph & David Bailey. (2014). Phenotypic screening in cancer drug discovery — past, present and future. *Nature Reviews Drug Discovery* 13, 588

15. Julia R. Pon1 and Marco A. Marra. (2015). Driver and Passenger Mutations in Cancer. *Annual Review of Pathology: Mechanisms of Disease*. 10, 25
16. Katrin Talkenberger; Elisabetta Ada Cavalcanti-Adam, Anja Voss-Böhme & Andreas Deutsch. (2017). Amoeboid-mesenchymal migration plasticity promotes invasion only in complex heterogeneous microenvironments. *Sci. Reports*. 9237
17. Keita Uchino, Takahiro Ochiya, Fumitaka Takeshita; RNAi Therapeutics and Applications of MicroRNAs in Cancer Treatment. *Japanese Journal of Clinical Oncology*. 2013, 43, 569
18. Khushwant S. Bhullar, Naiara Orrego Lagarón, Eileen M. McGowan, Indu Parmar, Amitabh Jha, Basil P. Hubbard, and H. P. Vasantha Rupasinghe. (2018). Kinase-targeted cancer therapies: progress, challenges and future directions. *Mol. Cancer*. 17:48
19. Kuhlow D, Florian S, von Figura G, Weimer S, Schulz N, Petzke KJ, Zarse K, Pfeiffer AF, Rudolph KL, Ristow M. (2010). Telomerase deficiency impairs glucose metabolism and insulin secretion. *Aging (Albany NY)*. 2:650-658
20. Maria Teresa Ventura, Marco Casciaro, Sebastiano Gangemi, and Rosalba Buquicchio. (2017). Immunosenescence in aging: between immune cells depletion and cytokines up-regulation. *Clin Mol Allergy*. 15: 21
21. Marko Ivancich, Zachary Schrank, Luke Wojdyla, Brandon Leviskas, Adijan Kuckovic, Ankita Sanjali, and Neelu Puri. (2017). Treating Cancer by Targeting Telomeres and Telomerase; *Antioxidants* 6, 15
22. Lowe SW1, Lin AW. (2000). Apoptosis in cancer. *Carcinogenesis*. 21(3):485-95
23. Martínez P, Blasco MA. (2017). Telomere-driven diseases and telomere-targeting therapies. *J Cell Biol*. 216, 875
24. Masood A. Shamas. (2011). Telomeres, lifestyle, cancer, and aging. *Curr Opin Clin Nutr Metab Care* 14, 28
25. Mohammad A. Jafri1, Shakeel A. Ansari1, Mohammed H. Alqahtani1 and Jerry W. Shay. (2016). Roles of telomeres and telomerase in cancer, and advances in telomerase-targeted therapies. *Genome Medicine* 8:69
26. Nicolo Riggi, Michel Aguet, and Ivan Stamenkovic. (2018). Cancer Metastasis: A Reappraisal of Its Underlying Mechanisms and Their Relevance to Treatment. *Annu. Rev. Pathol. Mech. Dis* 13:117
27. Norbury CJ1, Hickson ID. (2001). Cellular responses to DNA damage. *Annu Rev Pharmacol Toxicol*. 41:367-401
28. N. V. Krakhmal, M. V. Zavyalova, E. V. Denisov, S. V. Vtorushin, V. M. Perelmuter. (2015). Cancer Invasion: Patterns and Mechanisms. *Acta Naturae*. 7, 17
29. Prasad, R., Pal, D. & Mohammad, W. (2020). Therapeutic Targets in Telomerase and Telomere Biology of Cancers. *Ind J Clin Biochem*. 35, 135–146

30. Prem Prakash Kushwaha, Sanjay Gupta, Atul Kumar Singh and Shashank Kumar. (2019) Emerging Role of Migration and Invasion Enhancer 1 (MIEN1) in Cancer Progression and Metastasis. *Front. Oncol* 9, Article 868
31. Qi Zhang, Nak-Kyoon Kim, and Juli Feigon. (2011). Architecture of human telomerase RNA. *PNAS* 108, 20325
32. Rafael Solana, Graham Pawelec. (2004). The Neuroendocrine Immune Network in Ageing. *NeuroImmune Biology*. 1567-7443
33. Raffaella Diotti and Diego Loayza. (2011). Shelterin complex and associated factors at human telomeres. *Nucleus* 2, 119
34. Sanjukta Mukherjee, Chikara Dohno, Kaori Asano, Kazuhiko Nakatani. (2016). Cyclic mismatch binding ligand CMBL4 binds to the 5'-T-3'/5'-GG-3' site by inducing the flipping out of thymine base. *Nucleic Acids Research* 44, 7090
35. Sanjukta Mukherjee,* Chikara Dohno, Kazuhiko Nakatani*. (2017). Design and Synthesis of Cyclic Mismatch-Binding Ligands (CMBLs) with Variable Linkers by Ring-Closing Metathesis and their Photophysical and DNA Repeat Binding Properties. *Chem. Eur. J* 23, 11385
36. Sanjukta Mukherjee, Leszek Błaszczuk, Wojciech Rypniewski, Christoph Falschlunger, Ronald Micura, Asako Murata, Chikara Dohno, Kazuhiko Nakatani, and Agnieszka Kiliszek. (2019). Structural insights into synthetic ligands targeting A–A pairs in disease-related CAG RNA repeats. *Nucleic Acids Research* 47, 10906
37. Stephanie Wang, Chikezie O. Madu, Yi Lu. (2019). Telomere and Its Role in Diseases. *Oncomedicine*. 4:1
38. Vijay Sekaran, Joana Soares, and Michael B. Jarstfer. (2014). Telomere Maintenance as a Target for Drug Discovery. *J Med. Chem*. 57, 521
39. Weige Tan Bodu Liu Shaohua Qu Gehao Liang Wei Luo Chang Gong. (2018) MicroRNAs and cancer: Key paradigms in molecular therapy. *Oncology Letters* 15, 2735
40. Yan Xu. (2011). Chemistry in human telomere biology: structure, function and targeting of telomere DNA/RNA. *Chem Soc Rev* 40, 2719
41. Yoo-Ah Kim, Dong-Yeon Cho, and Teresa M. Przytycka. (2016). Understanding Genotype-Phenotype Effects in Cancer via Network Approaches. *plos Comput Biol*. 12, e1004747